NASA TECHNICAL NOTE

NASA TN D-3947

NASA TN D-3947

TIME-DEPENDENT STRUCTURE OF ONE-DIMENSIONAL MAGNETIC COMPRESSION WAVES IN COLLISIONLESS PLASMAS

OBLIQUE AMBIENT MAGNETIC FIELD

by Vernon J. Rossow

Ames Research Center
Moffett Field, Calif.

NATIONAL AERONAUTICS AND SPACE ADMINISTRATION • WASHINGTON, D. C. • MAY 1967

NASA TN D-3947

TIME-DEPENDENT STRUCTURE OF ONE-DIMENSIONAL MAGNETIC COMPRESSION WAVES IN COLLISIONLESS PLASMAS

OBLIQUE AMBIENT MAGNETIC FIELD

By Vernon J. Rossow

Ames Research Center
Moffett Field, Calif.

NATIONAL AERONAUTICS AND SPACE ADMINISTRATION

For sale by the Clearinghouse for Federal Scientific and Technical Information
Springfield, Virginia 22151 – CFSTI price $3.00

TIME-DEPENDENT STRUCTURE OF ONE-DIMENSIONAL MAGNETIC COMPRESSION WAVES IN COLLISIONLESS PLASMAS - OBLIQUE AMBIENT MAGNETIC FIELD

By Vernon J. Rossow

Ames Research Center

SUMMARY

Numerical analysis is made of the structure of one-dimensional unsteady magnetic compression waves propagating into collisionless plasmas when the ambient magnetic field is oblique to the wave direction. In the cases studied, both the subcritical and supercritical solutions changed continuously from one limiting situation to the other. A similarity rule was found for correlating the subcritical cases so that the two-parameter family of solutions in mass ratio and field angle were reduced to a single set.

INTRODUCTION

Recent studies of compression waves propagating through collisionless, completely ionized gases indicate that a large variety of wave shapes is possible. Such analyses bring about an understanding of these waves, and hopefully, a compilation of the many possible situations will help the experimenter identify the origin of probe data obtained in space or in the laboratory. With such considerations as motivation, the present study was carried out to find the structure of one-dimensional unsteady magnetic compression waves moving into a two-component, completely ionized plasma that is, in turn, embedded in a magnetic field. The initially cold plasma is compressed by a magnetic field that is driven by an electric field (the left boundary in fig. 1). The magnetic field in the undisturbed plasma has two constant components B_{xo} and B_{zo}, with $\tan \theta = B_{zo}/B_{xo}$. It is assumed that the flow field can be rotated about the x axis to eliminate any y component of the ambient magnetic field. The disturbance field, E_y, at the initiation plane causes the magnetic piston to be composed of only B_z and thereby imposes a restriction on the possible orientations between ambient and disturbance fields. In general, the compressed layer will involve all three components of the magnetic field and of the velocity vector. Of particular interest here is the variation in the structure of the compressed layer as the angle θ between the direction of wave propagation and the ambient magnetic field is changed from the alined ($\theta = 0^\circ$) to the transverse ($\theta = 90^\circ$) situation.

The structure of a single or solitary wave has been treated by Adlam and Allen (ref. 1) for a wave traveling perpendicularly to the ambient magnetic field and by Saffman (ref. 2) and Pataraya (ref. 3) for a wave moving along

the field lines. The results for the two limiting cases were generalized by Saffman (ref. 4) and Kellogg (ref. 5) to the cases where the propagation direction is at an arbitrary angle to the ambient magnetic field. Rather than just a single pulse, the general case consists of a group of pulses that may or may not be stable (refs. 4 and 5). Morton (ref. 6) studied the development with time of a one-dimensional compressed layer brought about by a magnetic piston moving at any angle relative to the undisturbed magnetic field direction. He found by an approximate treatment that the structure of the wave changes rather abruptly near the transverse limit when the mass ratio $R = m_i/m_e$ is large. For stronger waves, his more exact results obtained by numerical integration of the equations indicate that the change was not so abrupt as first thought; consequently, results near $\theta = 90^\circ$ resemble those at 90°.

The present investigation first supplements the work of Morton (ref. 6) by redoing the so-called subcritical waves[1] by the method of Auer, Hurwitz, and Kilb (refs. 7 and 8). Morton's results are then extended by new results, found by the present technique, for the supercritical case in which breaking occurs and wherein volume elements of plasma interchange positions during the event on a scale comparable with the size of the compressed layer. Both the present analysis and that of Morton start with the same basic equations but differ in the manner of solution. Whereas Morton used a continuum formulation with an artificial viscosity in the numerical work, here Lagrangian coordinates are used to follow the plasma elements in order to integrate the time-dependent flow field. Such a discrete model permits the calculation to proceed through breaking of the waves and interchanging of particles without requiring more assumptions as to the nature of the process.

DEVELOPMENT OF EQUATIONS FOR NUMERICAL ANALYSIS

Introducing the longitudinal (B_{xo}) in addition to the transverse component (B_{zo}) of the magnetic field causes the three velocity components to be coupled to each other through the electromagnetic fields. As a result, the procedure used here differs from that of Auer, Hurwitz, and Kilb (refs. 7 and 8) only in that more components of the various quantities must be carried along in the analysis. A brief description of the equations leading to the numerical work will be given in this section and emphasis will be given to the new material.

In vector notation, the equations for conservation of mass and momentum of the ions (subscript i) and of the electrons (subscript e) for the planar flow field under consideration are

---

[1]Convention has defined subcritical compression waves as those in which the plasma elements retain their original order. By contrast, supercritical waves are those wherein the wave intensity is so large that plasma elements exchange positions on a large scale so that the structure of the compressed layer is irregular. When $\theta = 90^\circ$, the division between the two types of waves occurs at an Alfvén Mach number of 2.0;

$$\text{Alfvén Mach number} = M_A = U_{wave}/\{B_o/[\mu n_o(m_e + m_i)]^{1/2}\}$$

$$\frac{\partial n_{i,e}}{\partial t} + \frac{\partial n_{i,e} u_{i,e}}{\partial x} = 0 \tag{1}$$

$$\frac{\partial \underset{\sim}{U}_{i,e}}{\partial t} + u_{i,e} \frac{\partial \underset{\sim}{U}_{i,e}}{\partial x} = \pm \frac{e}{m_{i,e}} (\underset{\sim}{E} + \underset{\sim}{U} \times \underset{\sim}{B}) \tag{2}$$

since all the derivatives with respect to y and z are zero and the ions are singly ionized. The quantities $n_{i,e}$, $m_{i,e}$ are the number density and mass of the ions and electrons, respectively, and the velocity is $\underset{\sim}{U} = \hat{i}u + \hat{j}v + \hat{k}w$. Similarly, the electromagnetic field equations for the one-dimensional wave system are

$$\frac{\partial B_x}{\partial x} = 0 \tag{3}$$

$$\frac{\partial E_x}{\partial x} = \frac{e}{\epsilon} (n_i - n_e) \tag{4}$$

$$\nabla \times \underset{\sim}{B} = e\mu(n_i \underset{\sim}{U}_i - n_e \underset{\sim}{U}_e) \tag{5}$$

$$\nabla \times \underset{\sim}{E} = - \frac{\partial \underset{\sim}{B}}{\partial t} \tag{6}$$

where the displacement current has been assumed to be negligible. Since the plasma frequency is many orders of magnitude greater than any of the cyclotron frequencies, the number density of ions and electrons are taken to be equal as a first approximation (ref. 9). Therefore,

$$n_i = n_e \equiv n \quad \text{and} \quad u_i = u_e \equiv u \tag{7}$$

As in previous analyses (refs. 7 and 8), the electrons are assumed to retain their original order while the ions are permitted to take any order that their dynamics might dictate. Justification for this approximation is given in reference 9.

As an aid in the numerical work, the magnetic vector potential, $\underset{\sim}{A}$, and the electric potential, φ, are introduced such that

$$\underset{\sim}{B} = \nabla \times \underset{\sim}{A} \quad \text{and} \quad \underset{\sim}{E} = - \frac{\partial \underset{\sim}{A}}{\partial t} - \nabla\varphi$$

For the one-dimensional unsteady problem being treated here,

$$E_x = - \frac{\partial \varphi}{\partial x} ; \qquad E_y = - \frac{\partial A_y}{\partial t} ; \qquad E_z = - \frac{\partial A_z}{\partial t} \tag{8a}$$

$$B_x = \frac{\partial A_z}{\partial y} = B_{xo} = \text{constant} ; \qquad B_y = - \frac{\partial A_z}{\partial x} ; \qquad B_z = \frac{\partial A_y}{\partial x} \tag{8b}$$

These equations can be integrated to yield

$$A_y(x,t) = \int_o^x B_z(x_1,t)dx_1 - \int_o^t E_y(0,t_1)dt_1 + C_y \tag{9a}$$

$$A_z(x,t) = -\int_o^x B_y(x_1,t)dx_1 - \int_o^t E_z(0,t_1)dt_1 + C_z + yB_{xo} \tag{9b}$$

where the constants C_y and C_z are determined by conditions at the reflection or right side of the flow field. The quantity yB_{xo} is added to complete the definition of the magnetic vector potential and does not enter the analysis because the y coordinate can be ignored.

Before the differential equations can be further adapted to their difference form for the numerical calculations, the initial conditions (i.e., at $t = 0$) and the restrictions at the boundaries $x = 0$ and $x = x_m$ need to be specified. As assumed by Auer, Hurwitz, and Kilb (refs. 7 and 8) and by Morton (ref. 6), the particles are taken to be cold and therefore stationary at $t = 0$ with uniform distribution throughout the flow field. The magnetic field in the undisturbed plasma has the two constant components B_{xo} and B_{zo} (see fig. 1). At the initiation plane, the disturbance to the plasma is assumed to be brought about by an electric field in the y direction

$$E_y(0,t) = E_{yo}(1 - e^{-\alpha t}) \; ; \qquad E_z(0,t) = 0 \tag{10}$$

that generates a magnetic field in the z direction. (The time-rise factor α was always taken to be 0.12 in the calculation.) This magnetic field forces the plasma away from the left boundary with a piston-type action so that a wave field and compressed layer are produced. It is assumed that the reflection plane at $x = x_m$ is impermeable to both the magnetic field and the plasma so that all disturbances are reflected without loss. The magnetic vector potentials there are taken as $A_y(x_m,t) = A_z(x_m,t) = 0$ so that $C_y = -x_m B_{zo}$ and $C_z = x_m B_{yo} = 0$ in equations (9).

With these quantities as starting conditions, the y and z momentum equations for the ions and electrons can be integrated along the particle paths to yield

$$v_i + \frac{eA_y}{m_i} = \frac{eA_y^{o+}}{m_i} + \frac{eB_{xo}}{m_i} z_i \tag{11a}$$

$$v_e - \frac{eA_y}{m_e} = -\frac{eA_y^{o-}}{m_e} - \frac{eB_{xo}}{m_e} z_e \tag{11b}$$

$$w_i + \frac{eA_z}{m_i} = \frac{eA_z^{o+}}{m_i} - \frac{eB_{xo}}{m_i} y_i \tag{11c}$$

$$w_e - \frac{eA_z}{m_e} = -\frac{eA_z^{o-}}{m_e} + \frac{eB_{xo}}{m_e} y_e \tag{11d}$$

where the velocities are zero at $t = 0$ and the superscripts on A designate the value of the magnetic vector potential at the location of the particle at $t = 0$.

Capital letters are now used to designate the variables in dimensionless form where the reference length, time, velocity, etc., are given by

$$\lambda = U_A/\omega_{ch}$$

$$t^* = \lambda/U^*$$

$$U^* = (U_A U_D)^{1/2}$$

$$V^* = W^* = (m_i + m_e)U^*/(m_i m_e)^{1/2}$$

$$B^* = B_o U^*/U_A$$

$$A^* = \lambda B^*$$

with $B_o = (B_{xo}^2 + B_{zo}^2)^{1/2}$, $U_A = B_o/[\mu n_o(m_i + m_e)]^{1/2}$, $U_D = E_{yo}/B_o$, and $\omega_{ch} = eB_o/(m_i m_e)^{1/2}$. The dimensionless variables then become $U = u/U^*$, $BY = B_y/B^*$, $AY = A_y/A^*$, $X = x/\lambda$, $T = t/t^*$, etc., and the mass ratio is defined as $R = m_i/m_e$. It is also convenient to introduce the Lagrangian variable, ξ, so that

$$\xi = \int_o^X \frac{n}{n_o}\, dX_1$$

As was done previously, the flow field is divided into slabs of plasma, the thicknesses of which are then made vanishingly small. Each slab or sheet contains the same number of ions and electrons and is located at the mass center of the element it represents. The procedure used in reference 8 is used to set up an array of equations to find the motion of the slabs of plasma and the associated electromagnetic fields. Recursion relations used in the machine program to find the magnetic field components throughout the flow field are then found for the kth slab as (compare, e.g., with ref. 10)

$$BY_{k-1} - [2 + D(X_{k+1} - X_k)]BY_k + BY_{k+1} + HY_k = 0 \tag{12a}$$

$$BZ_{k-1} - [2 + D(X_{k+1} - X_k)]BZ_k + BZ_{k+1} + HZ_k = 0 \tag{12b}$$

where $D = X_m/N$ and

$$HY_k = \frac{D(BXO)}{R^{1/2}} [YI_{k+1} - YI_k + R(YE_{k+1} - YE_k)] \tag{13a}$$

$$HZ_k = \frac{D^2(BZO)}{R + 1} \frac{R + (AY_{k+1}^{O+} - AY_k^{O+})}{B_{zo}} + \frac{D(BXO)}{R^{1/2}} [ZI_{k+1} - ZI_k + R(ZE_{k+1} - ZE_k)] \tag{13b}$$

since $BY0 = 0$. This matrix is inverted for the magnetic field values by first calculating the quantities

$$RY_k = 1/[2 + D(X_{k+1} - X_k) - RY_{k+1}] \tag{14a}$$

$$SY_k = RY_k(SY_{k+1} + HY_k) \tag{14b}$$

$$RZ_k = 1/[2 + D(X_{k+1} - X_k) - RZ_{k+1}] \tag{14c}$$

$$SZ_k = RZ_k(SZ_{k+1} + HZ_k) \tag{14d}$$

starting at the reflection plane where $k = N$ and proceeding to the initiation plane magnetic piston region where $k = 1$. Since the boundary at X_m is a perfect reflector, the beginning values for $k = N$ are

$$RY_N = 1/[1 + 2D(X_m - X_N)]$$

$$SY_N = 0$$

$$RZ_N = 1/[1 + 2D(X_m - X_N)]$$

$$SZ_N = RZ_N(HZ_N)$$

Once these quantities are known, the recursion equations

$$BY_k = RY_k(BY_{k-1}) + SY_k \tag{15a}$$

$$BZ_k = RZ_k(BZ_{k-1}) + SZ_k \tag{15b}$$

yield the local magnetic field after the value at the initiation plane (and in the piston region) is determined by

$$BY_w = \frac{SY_1 - (BX0/R^{1/2})[R(YE_1) + YI_1]}{1 - RY_1 + D(X_1)} \tag{16a}$$

$$BZ_w = \frac{SZ_1 + D\left\{-AY_w + \frac{D(BZ0)}{R+1}\left[\frac{R-1}{2} - N(R+1) + \frac{AY^{0+}}{BZ0}\right] + \frac{BX0}{R^{1/2}}[R(ZE_1) + ZI_1]\right\}}{1 - RZ_1 + D(X_1)} \tag{16b}$$

where $AY_w = AY(0,T) = -[T + (e^{-\alpha T} - 1)/\alpha] - X_m(B_{z0})$, since $EY0 = 1$. The acceleration of the slabs of plasma is found by calculating the magnetic pressure difference on its two sides; that is,

$$\ddot{X}_k = -(BY_k^2 - BY_{k-1}^2 + BZ_k^2 - BZ_{k-1}^2)/2D \tag{17}$$

The accuracy of the numerical calculations can be monitored to a certain extent by checking to see whether the momentum and energy content of the entire flow field is conserved. The three components of the momentum are

evaluated by means of

$$2D \sum_{1}^{N} U_k = \int_{0}^{T} [BYW^2 + BZW^2 - BY_N^2 - BZ_N^2]dT_1 \tag{18a}$$

$$\sum_{1}^{N}[VE_k + R(VI_k)] = R^{1/2}BXO \sum_{1}^{N}(ZI_k - ZE_k) \tag{18b}$$

$$\sum_{1}^{N}[WE_k + R(WI_k)] = -R^{1/2}BXO \sum_{1}^{N}(YI_k - YE_k) \tag{18c}$$

An energy check during the calculations is made by evaluating and comparing the two sides of the expression

$$2\int_{0}^{T}(BZ_w)EY(0,T_1)dT_1 = D\sum_{1}^{N}\left[U_k^2 + (R+1)\left(VI_k^2 + WI_k^2 + \frac{VE_k^2 + WE_k^2}{R}\right)\right.$$

$$\left. + (X_{k+1} - X_k)(BY_k^2 + BZ_k^2)\right] \tag{19}$$

A machine program for solving the foregoing system of equations was used to find a number of solutions. Results from the computer were written on magnetic tape and then plotted electrically. Accuracy tests were carried out on various cases to determine which mesh sizes were most suitable.

RESULTS OF NUMERICAL ANALYSIS

Emphasis is first placed on the variation in the structure of the compressed layer as the angle θ between the wave direction and the ambient magnetic field changes from alined (0^o) to normal (90^o) incidence. The effect of mass ratio on the solution is then considered for two situations: first, the ambient magnetic field is chosen to be 1.0 so that the compression wave is subcritical and the plasma sheets retain their original order, that is, $B_o = (BXO^2 + BZO^2)^{1/2} = 1.0 (M_A \approx 1.5)$; second, the structure is considered for $B_o = 0.2 (M_A \approx 5.8)$. For a wave of this strength, the plasma slabs interchange order on a large scale and a random irregular-type flow field results. All other factors in the calculations are held fixed as θ varies from 0^o to 90^o.

Subcritical Case

Data on the structure of a number of the subcritical cases are presented in figures 2 through 10. Of particular interest here is the manner in which the structure changes as the magnetic field angle, θ, or mass ratio, R, is varied. The growth of the compressed layer with time is shown in figures 4 through 10 for selected cases so that the reader can see how the flow field

shown in figures 2 and 3 developed. Variation of the velocity components with distance at a given time are presented in part (a) of each figure along with the magnetic field components. Special features of each solution are noted in the figure titles.

Figure 2 presents the structure of the compressed layer for $M_A \approx 1.5$ at several angles when the time T is 60, that is, 60 time units after the disturbance was initiated. At the mass ratio chosen, the flow field changes gradually from one type to another - the changeover appears to occur at about 60°. Although the calculations were not made specifically for comparison, the curves for the magnetic field intensities are in general agreement with the solutions of Kellogg (ref. 5) and Morton (ref. 6) and no striking disparities are noted.

Several changes in the flow field are observed as the angle of the ambient field varies. Because of the presence of a precursor-type wave, the compressed layer or disturbed region is thickest at $\theta = 0^\circ$ (see also figs. 5-9). Also apparent in figure 2 is the extent that the magnetic field associated with the disturbance diffuses into the compressed layer at $\theta = 0^\circ$ causing the piston region to be smaller there. In contrast, this mixing at the piston-compressed layer interface is only several units of λ at 90°.

Although most of the structures shown in figures 4 through 10 appear to have established a pattern, they may not have been fully developed when the calculations were terminated. (Machine storage capacity prevented an increase in the size of the flow field and, hence, in the running time. Had the present cases been carried further, excessive interference from the reflection plane would have resulted.) The rather abrupt appearance of the small wave sequence in the $\theta = 60^\circ$ case (see fig. 8(b)), at about $T = 35$, suggests that prolonged tests might have brought a new wave system to light in some of the other solutions. This does not seem likely though because the structure of the compressed layers appears to have settled down to a pattern.

Similarity Parameter for Subcritical Flow Fields

Whereas the subcritical cases for $\theta = 90^\circ$ are independent of the mass ratio R, all other angles are affected by it. Both Morton and Kellogg estimated that the flow field changes rapidly with angle near 90° when the mass ratio is large. In order to study the effect of R on the structure of the compressed layer, a sequence of runs was made for $\theta = 60^\circ$ and the results at $T = 60$ are presented in figure 3. Although nothing new appeared the structure changed considerably. Of most importance, however, is the resemblance between the three new solutions and the results for $\theta = 90^\circ$, 75°, and 45° in figure 2 (the 60° cases for $R = 25$ are duplicates). These results led the author to find an empirical rule for relating one case to another and then to the justification of the results by means of the equations. A best fit to the data in figures 2 and 3 was obtained with the rule

$$BZO_I = BZO_{II}$$

$$BXO_I^2(R_I^{1/2} - 1) = BXO_{II}^2(R_{II}^{1/2} - 1)$$

where I and II are the two cases being related by the rule. However, an examination of the recursion equations and, in particular, the quantities HY and HZ (eqs. (13)) led to the similarity parameter that is felt to be the correct one.

$$BZO_I = BZO_{II} \tag{20a}$$

$$BXO_I^2(R_I^{1/2} - R_I^{-1/2}) = BXO_{II}^2(R_{II}^{1/2} - R_{II}^{-1/2}) \tag{20b}$$

The two forms are equal at $R = 1$ and become equivalent at large mass ratios since $R^{1/2} - 1 = (R - 1)/(R^{1/2} + 1) \approx (R - 1)/R^{1/2}$. Equation (20a) arises from the fact that the solutions at 90° are independent of R as long as the plasma slabs do not interchange order. Equation (20b) is justified by considering the lateral displacements of the particles in the two cases as they appear in equations (13). Since the mass of the electron is the same for both cases, the relative lateral displacement is reduced by an increase in BXO, so that, for example,

$$Z_e \approx -\text{constant}/BXO$$

Lateral movement of the ion is approximated by

$$Z_i \approx +(R\ \text{constant})(1/R) = \text{constant}/BXO$$

The first term describes the effect on the Larmor radius brought about by the longitudinal magnetic field and mass of the ion and the second term treats the reduced acceleration (and, hence, lower velocity and distance) for a heavier ion. Hence, the ion and electron have the same proportionality factor but have opposite signs. When these results are inserted into the last term of equations (13), which involves $BXO/R^{1/2}$, the similarity rule presented in equations (20) is derived.

As a test of the similarity rule (20), two sets of related cases were calculated and the results are compared in figure 4 at three time intervals. Exact correspondence is not achieved, but the general features of the magnetic field lines are reproduced quite well considering the large difference in mass ratio between the cases compared. As is to be expected, the other flow-field parameters deviate more from each other. A horizontal line for the piston region on BZ was omitted to illustrate the difference in the motion of the interface. It appears that the average velocity is about the same for the cases compared but the heavier ions oscillate at a lower frequency and greater amplitude than the lighter ions. The high frequency oscillations of the lighter ion are not duplicated (fig. 5(b)) by the heavier ion. As a result, the magnetic field of case III ($R = 1836$) appears to be a mean of case IV ($R = 25$). From these results, the similarity rule, equations (20), appears to give satisfactory similar solutions.

Supercritical Flow Fields

The variation of the magnetic field components in the compressed layer for a disturbance of supercritical strength is first illustrated in figure 11 for several values of θ from 0° to 90°. Once again, the structure does not change abruptly from one form to the other. Transition from the 0° pattern to the type typical of the transverse situation occurs at about 30°. The formation of a region of nearly uniform magnetic field near the piston also appears to be characteristic of the solutions near 0°. As θ increases from about 30°, the extent of this area decreases quickly to zero. Since $BZ)_{piston}$ and the length of the piston region are essentially independent of θ, the uniform compressed layer near the piston for $\theta = 0^\circ$ and 15° does not appear to be caused by diffusion of the disturbance magnetic field into the compressed layer. It may be the beginning of the formation of a uniform compressed layer, in which case, the forward part of the layer could be considered as the shock structure (in a gasdynamic continuum sense). The calculations could not be carried further to see if this were true. Whether the depth of the compressed layer is a function of θ cannot be judged from figure 11 because of the unsteady nature of the supercritical cases. Disturbances at X = 140 to 160 for the $\theta = 15^\circ$ solution result from particles thrown far ahead of the compressed layer by the start-up of the piston field. Forward spraying of the particles occurs in most of the strong or supercritical solutions but such plasma motion is not always as apparent in the magnetic field profiles as exhibited for $\theta = 15^\circ$ in figure 11. Although the z component of the magnetic field exhibits a random profile of about the same magnitude at all angles, the intensity of the y component decreases regularly from 0° to 90°. For angles of 45° and above, the magnitude of BY relative to BZ appears to be the most obvious indication of the obliqueness of the ambient field.

The influence of the mass ratio on the wave structure is shown in figure 12 for $\theta = 60^\circ$. This angle was chosen to parallel the subcritical solutions. Note that the magnetic profiles do not change with R in quite so pronounced a fashion as did the subcritical cases in figure 3. A slight increase in the size of the disturbed region for R = 100 is attributed to the unsteady character of the flow field and not to an increased average growth rate. These solutions have the same irregular shape as those in figure 11, but they do not resemble any of them closely enough to form a correlation. In particular, the time and distance dilation formula derived empirically by Auer, Hurwitz, and Kilb (ref. 8) for the 90° supercritical waves does not apply for any other angle because the depth of the compressed layer does not change with R. Attempts were made to arrive at some sort of similarity rule for these results, but no satisfactory parameter was found.

As was done for the subcritical cases, the development with time is shown for several cases in figures 13 through 17. Special features of the solutions are again noted in the figure titles.

CONCLUDING REMARKS

Calculations of the flow field generated in a collisionless plasma by a disturbance of the magnetic piston type yielded results that agree in general with previous work on oblique magnetic compression waves. The structure changed continuously with angle from one limiting form to the other, that is, from 0° to 90°. Although the solutions at intermediate values of θ are more complex in their dependence on mass ratio than the results at 90°, a similarity rule was found for subcritical wave speeds. This rule makes it possible to relate magnetic field results at one mass ratio and angle to a corresponding one, thereby reducing a two-parameter family to a single set. A comparable rule was not found for the supercritical flow fields. The need for such a rule is not so great because the solutions do not depend strongly on mass ratio.

Limitations imposed by computer capacity did not permit the calculations to be carried out as far as desirable in all cases. Although it does not seem likely, some of the foregoing conclusions might have been different had the flow field been allowed to develop for a sufficiently longer period. Also, it should be remembered that the disturbance used to generate the wave was an electric field in the y direction at the initiation plane. Such a field produces a magnetic piston composed of B_z only. Another type of piston might yield quite different results.

Ames Research Center
National Aeronautics and Space Administration
Moffett Field, Calif., 94035, Feb. 2, 1967
129-02-03-03-00-21

REFERENCES

1. Adlam, J. H.; and Allen, J. E.: The Structure of Strong Collision-Free Hydromagnetic Waves. Phil. Mag., 8th ser., vol. 3, no. 29, May 1958, pp. 448-455.

2. Saffman, P. G.: Propagation of a Solitary Wave Along a Magnetic Field in a Cold Collision-Free Plasma. J. Fluid Mech., vol. 11, pt. 1, Aug. 1961, pp. 16-20.

3. Pataraya, A. D.: Structure of Solitary Waves Propagated Along a Magnetic Field. Soviet Phys.-Tech. Phys., vol. 8, no. 11, May 1964, pp. 979-980.

4. Saffman, P. G.: On Hydromagnetic Waves of Finite Amplitude in a Cold Plasma. J. Fluid Mech., vol. 11, pt. 4, Dec. 1961, pp. 552-566.

5. Kellogg, Paul J.: Solitary Waves in Cold Collisionless Plasma. Phys. Fluids, vol. 7, no. 10, Oct. 1964, pp. 1555-1571.

6. Morton, K. W.: Finite Amplitude Compression Waves in a Collision-Free Plasma. Phys. Fluids, vol. 7, no. 11, Nov. 1964, pp. 1800-1815.

7. Auer, P. L.; Hurwitz, H., Jr.; and Kilb, R. W.: Low Mach Number Magnetic Compression Waves in a Collision-Free Plasma. Phys. Fluids, vol. 4, no. 9, Sept. 1961, pp. 1105-1121.

8. Auer, P. L.; Hurwitz, H., Jr.; and Kilb, R. W.: Large-Amplitude Magnetic Compression of a Collision-Free Plasma. II. Development of a Thermalized Plasma. Phys. Fluids, vol. 5, no. 3, Mar. 1962, pp. 298-316.

9. Rossow, V. J.: Magnetic Compression of Collision-Free Plasmas With Charge Separation. Phys. Fluids, vol. 8, no. 2, Feb. 1965, pp. 358-366.

10. Jones, Wm. Prichard; and Rossow, V. J.: Graphical Results for Large-Amplitude Unsteady One-Dimensional Waves in Magnetized Collision-Free Plasmas With Discrete Structure. NASA TN D-2536, 1965.

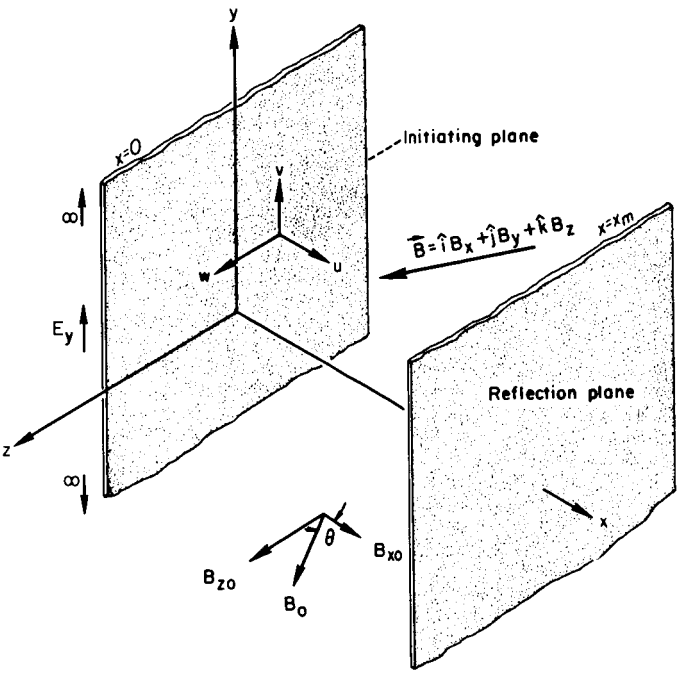

Figure 1.- Schematic diagram of flow field.

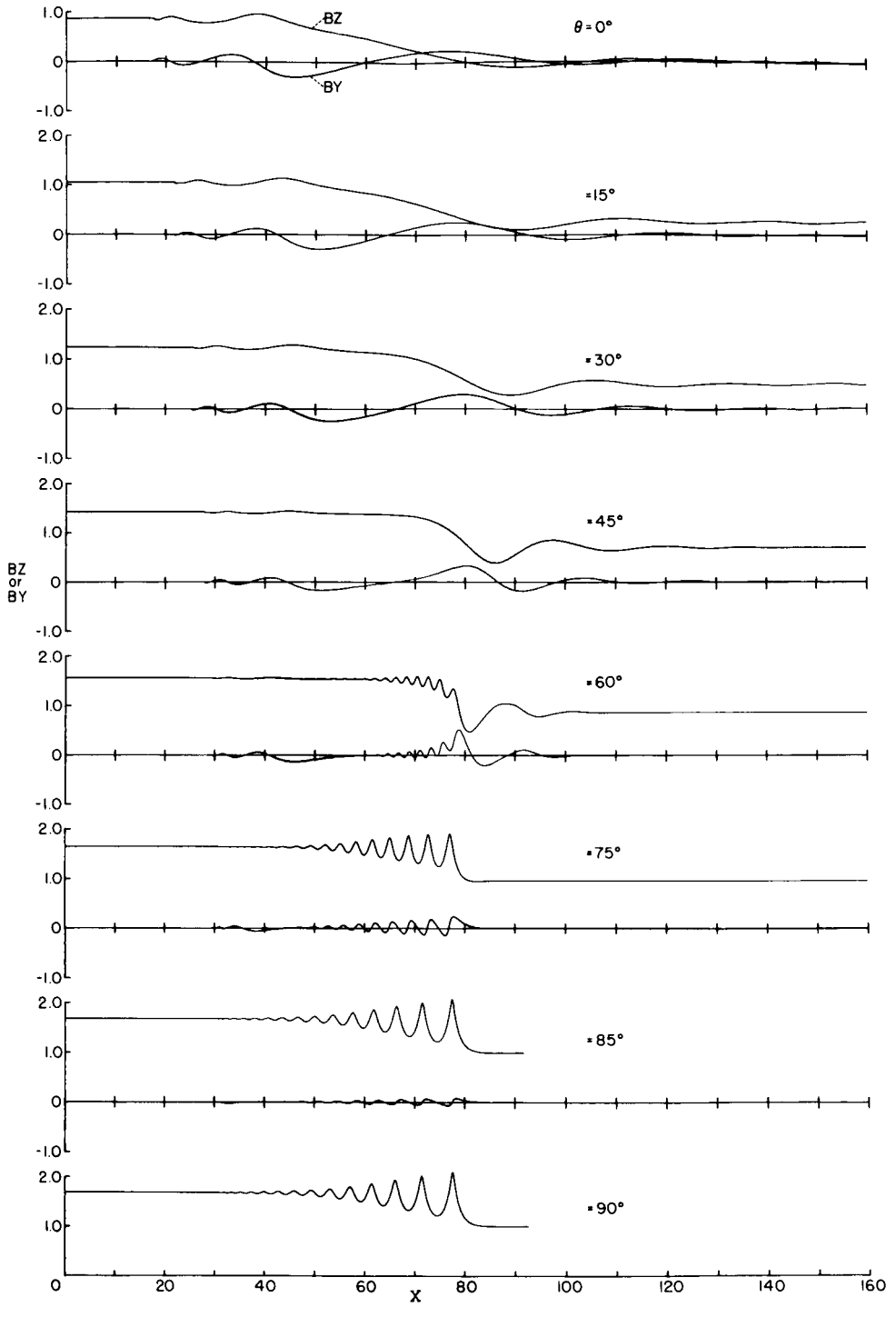

Figure 2.- Structure of compressed layer for subcritical disturbance at several values of magnetic field angle; R = 25, T = 60, B_o = 1.0 ($M_A \approx 1.5$).

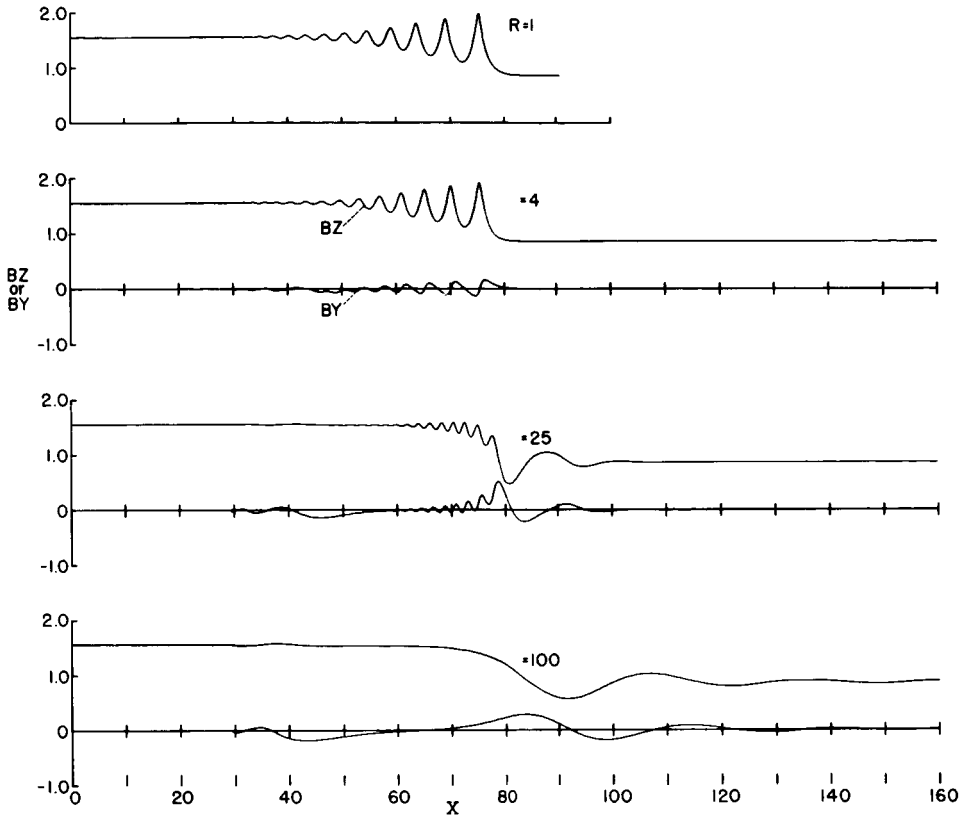

Figure 3.- Structure of compressed layer for subcritical disturbance for various mass ratios; $\theta = 60^{\circ}$, $B_o = 1.0$, T = 60.

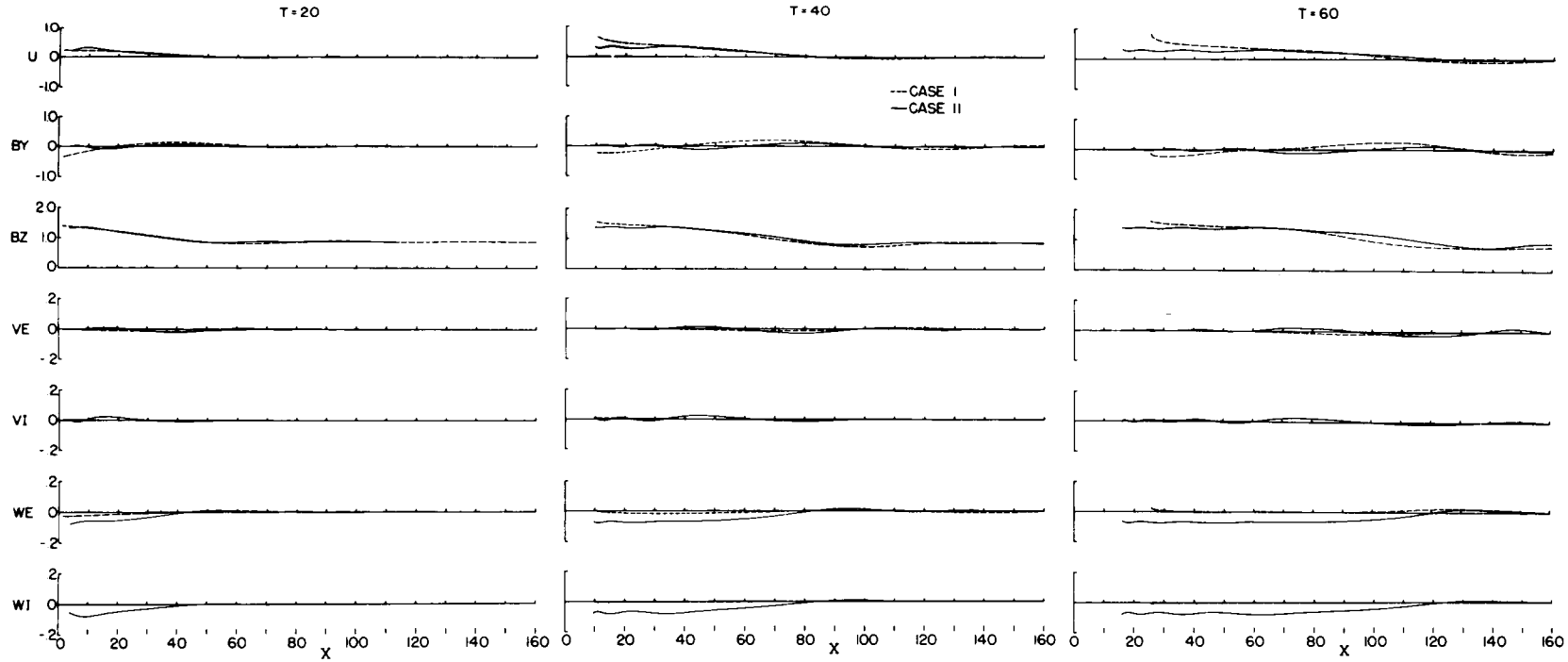

(a) $BX0^2(R^{1/2} - R^{-1/2}) = 10.706$; Case I: R = 1836, BX0 = 0.50, BZ0 = 0.866, B_o = 1.00, $\theta = 60^o$; Case II: R = 25, BX0 = 1.4935, BZ0 = 0.866, B_o = 1.7264, $\theta = 30.1^o$.

Figure 4.- Comparison of two test cases as predicted by similarity rule.

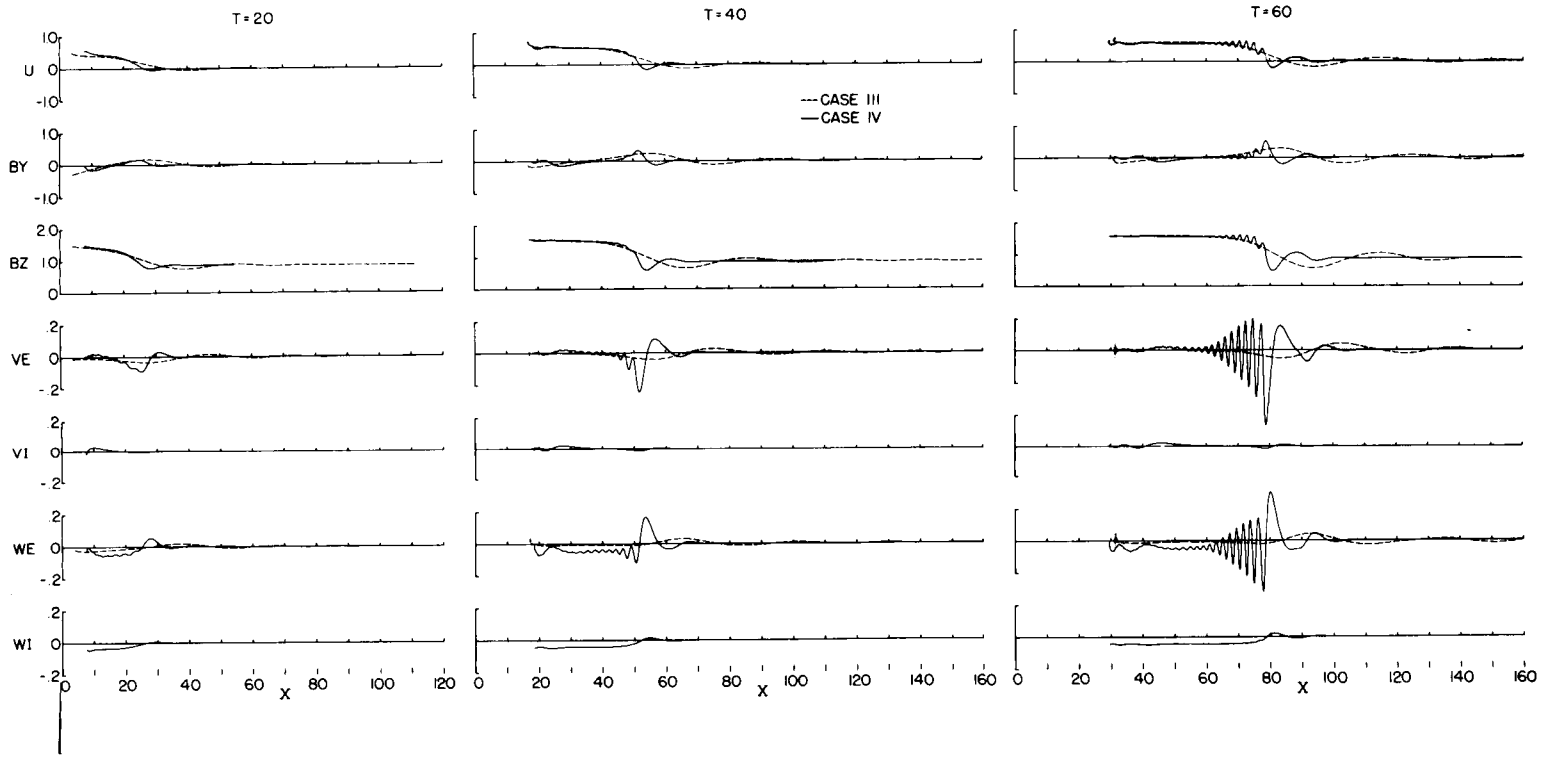

(b) $BX0^2(R^{1/2} - R^{-1/2}) = 1.20$; Case III: R = 1836, BX0 = 0.1674, BZ0 = 0.866, B_o = 0.882, $\theta = 79.06^\circ$; Case IV: R = 25, BX0 = 0.500, BZ0 = 0.866, B_o = 1.0, $\theta = 60^\circ$.

Figure 4.- Concluded.

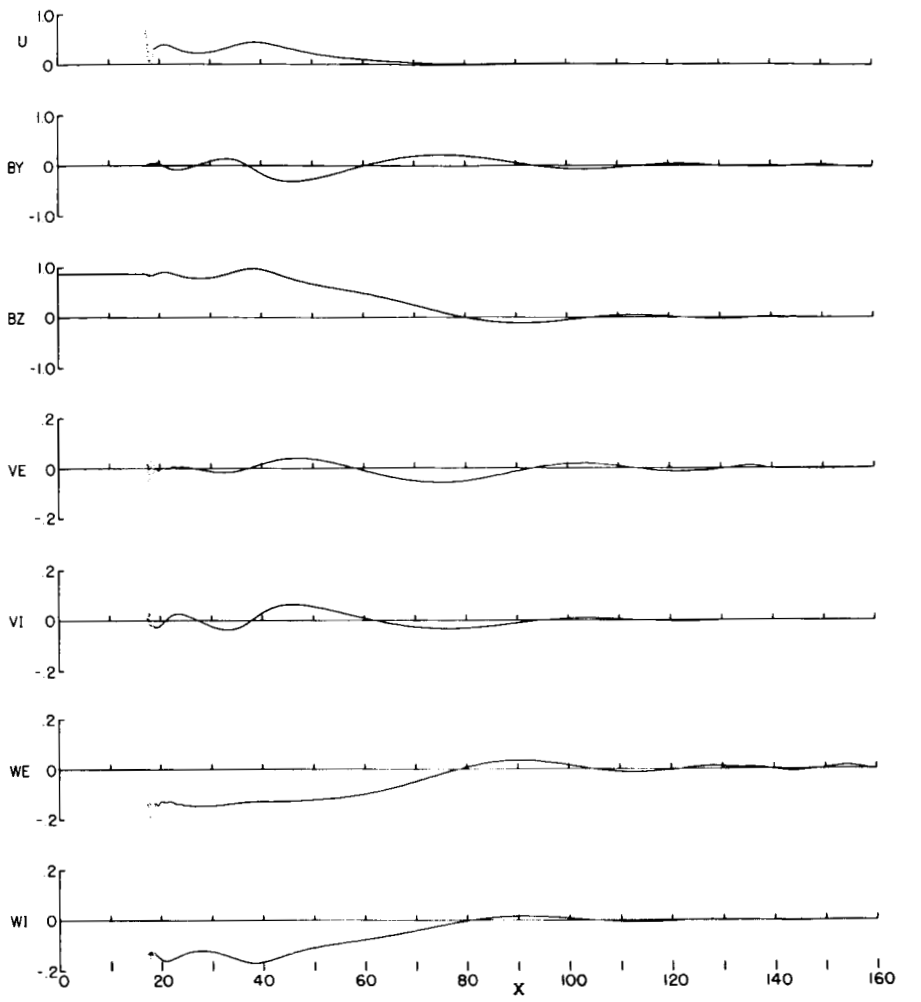

(a) Flow-field variables at T = 60. (Scatter in the data at the piston-plasma interface is characteristic of solutions near $\theta = 0^{\circ}$ and appears to result from an accumulation of plasma slabs at that location.)

Figure 5.- Structure of time-dependent flow field for subcritical wave; R = 25, $\theta = 0^{\circ}$, $B_o = 1.0$ (BX0 = 1.0, BZ0 = 0).

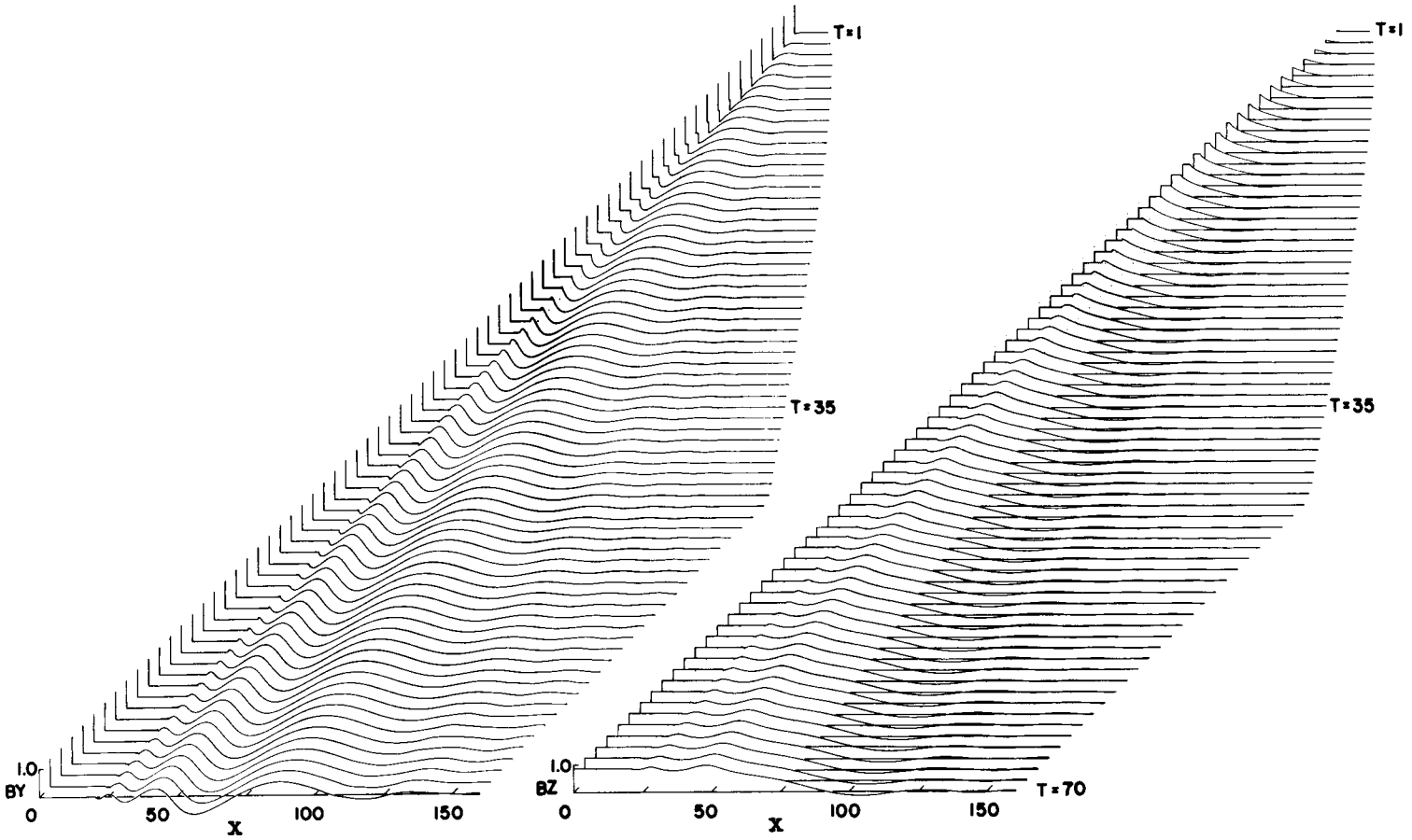

(b) Development of magnetic field components with time. (Note that since the disturbance electric field has only a y component, the driving or piston magnetic field contains only BZ so that the BY and BZ profiles are quite different.)

Figure 5.- Concluded.

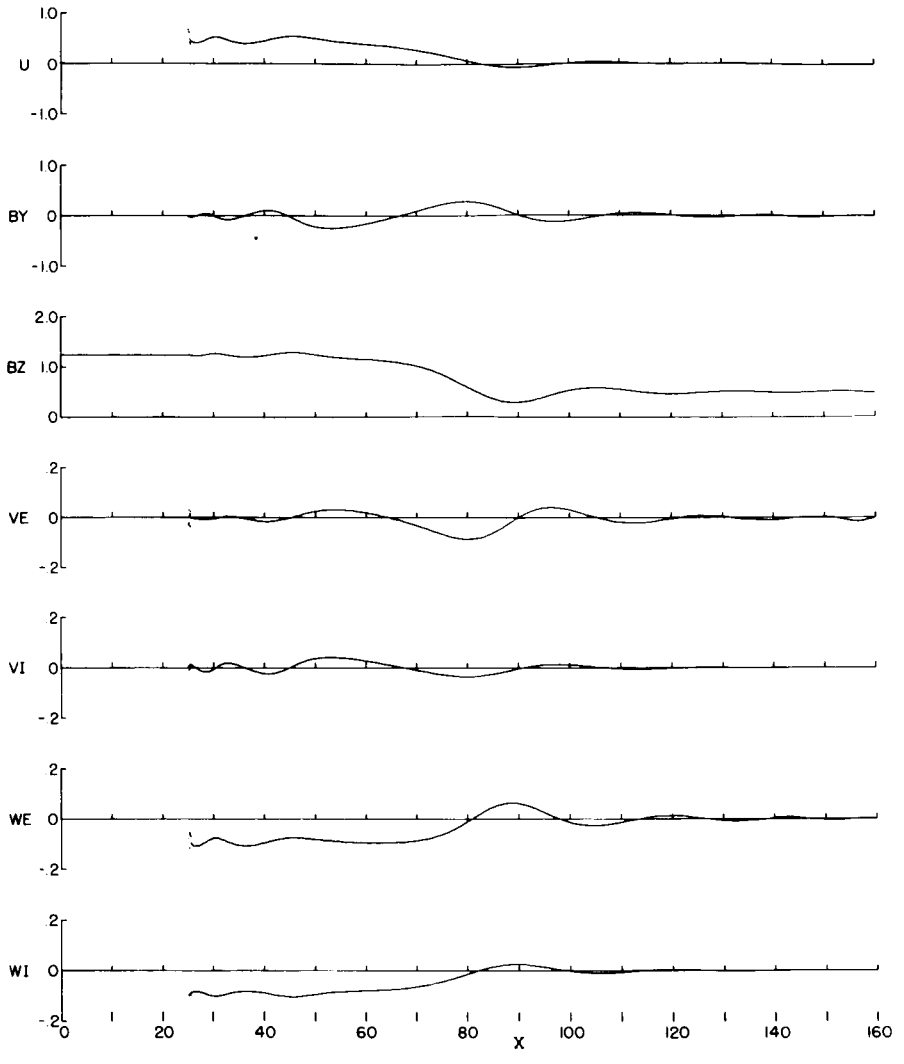

(a) Flow-field variables at $T = 60$. (About the only difference between this case and the one at $\theta = 0^{\circ}$ is the increased area under the BZ curve brought about by its present nonzero value in the ambient field.)

Figure 6.- Structure of time-dependent flow field for subcritical wave; $R = 25$, $\theta = 30^{\circ}$, $B_0 = 1.0$ (BX0 = 0.866, BZ0 = 0.500).

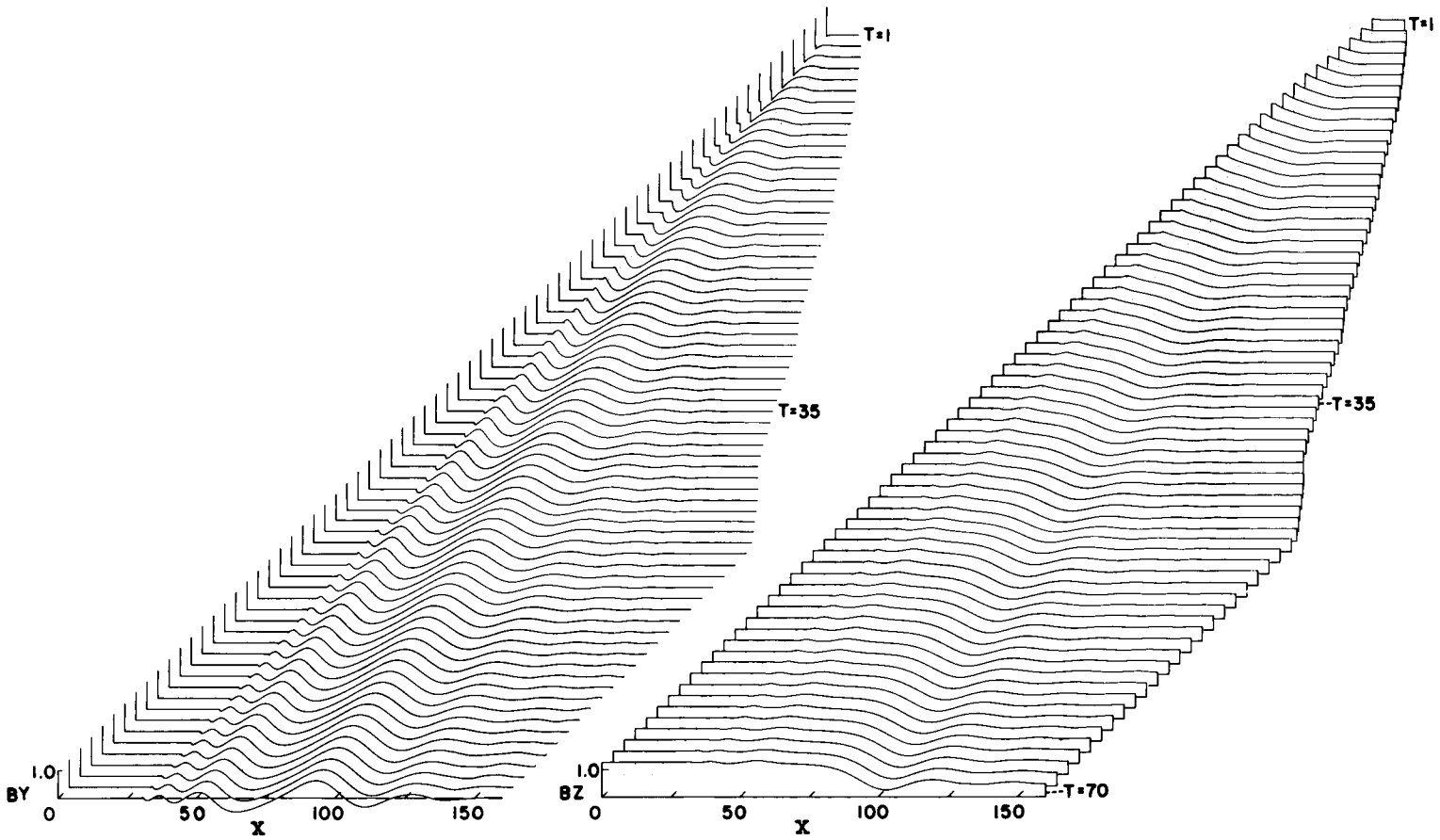

(b) Development of magnetic field components with time.

Figure 6.- Concluded.

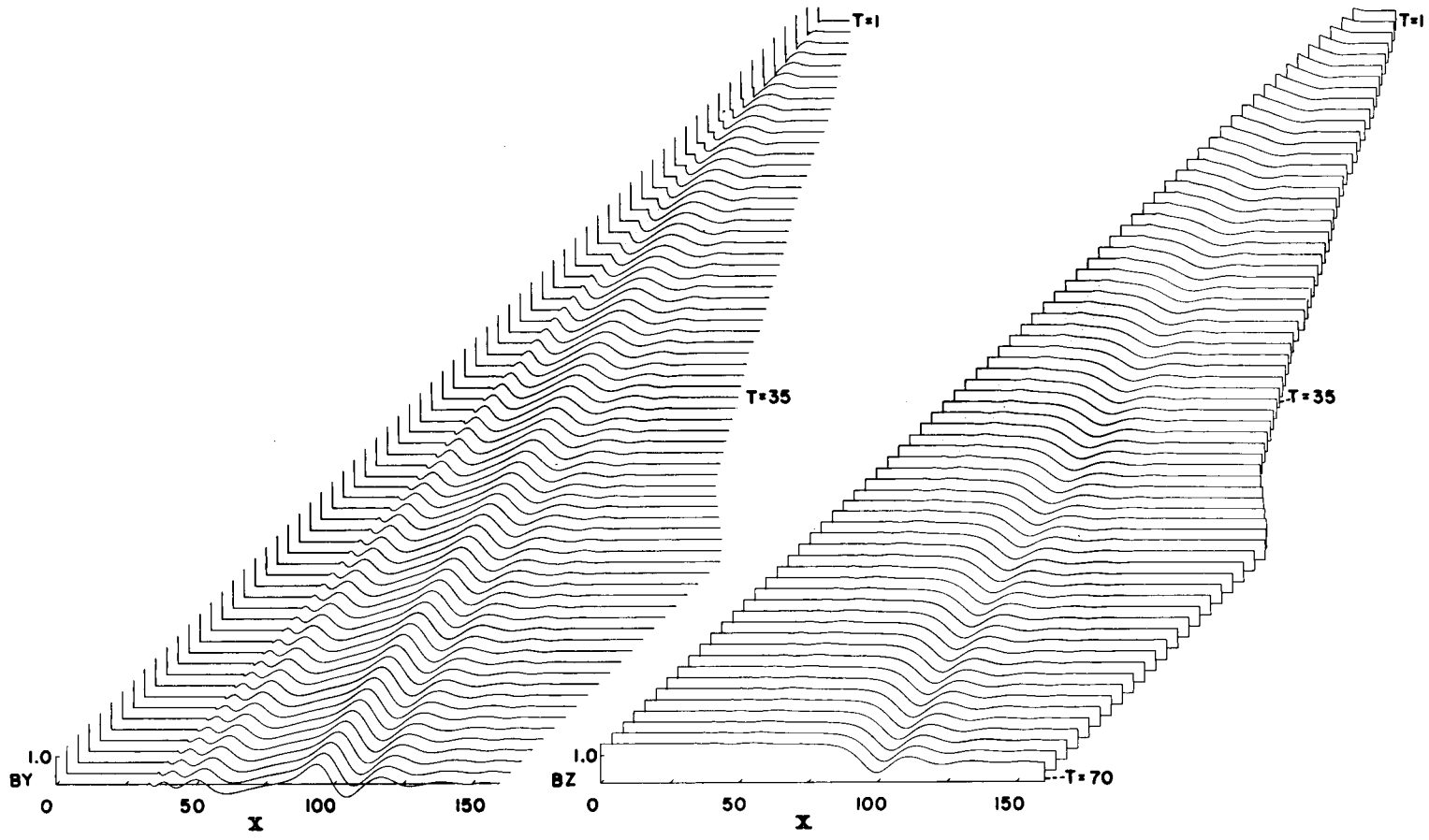

Figure 7.- Structure of time-dependent flow field for subcritical wave; R = 25, $\theta = 45^{\circ}$, $B_0 = 1.0$ (BX0 = 0.707, BZ0 = 0.707). (Profiles of the flow variables at T = 60 are not available because of difficulties with the computer program when this case was calculated. These results are presented because the BY field appears to be developing a sequence of separate (or solitary) wave trains similar to those discussed by Kellogg (ref. 5).)

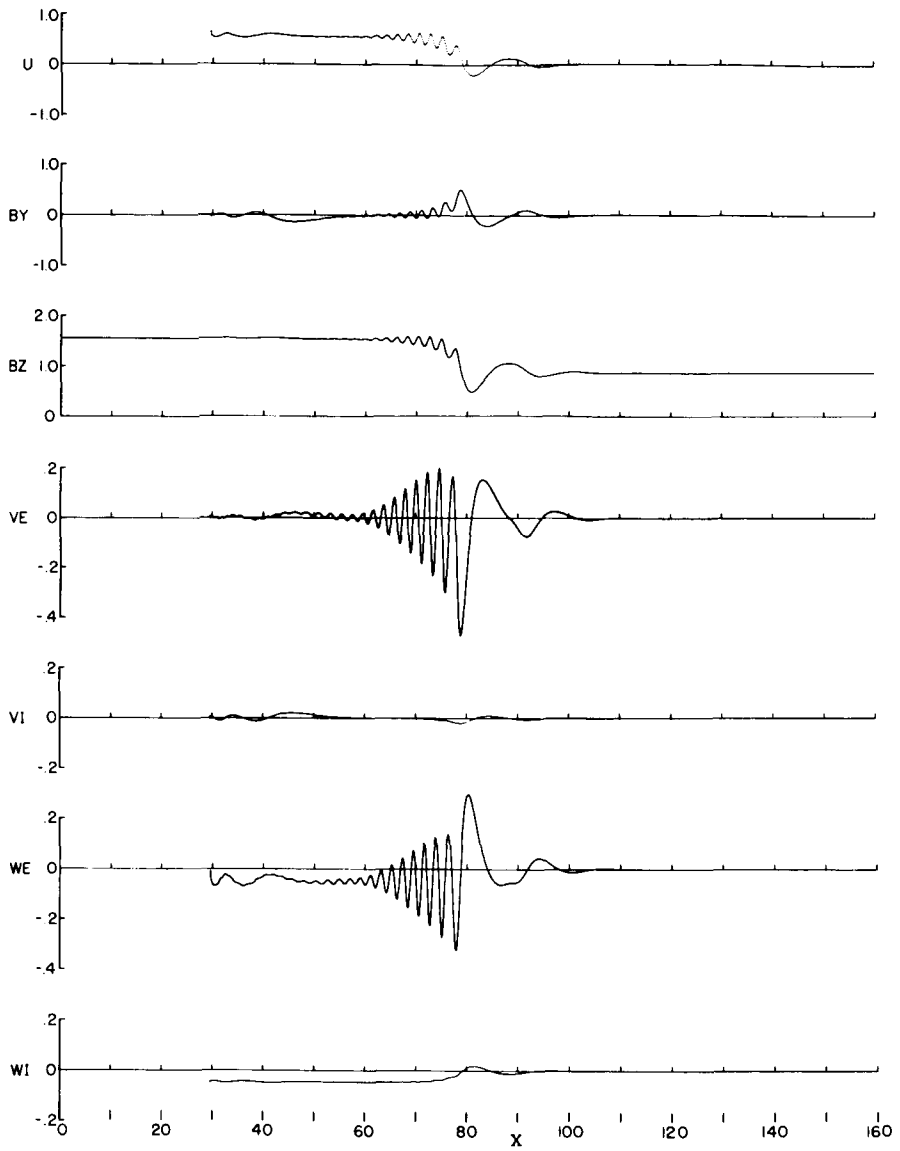

(a) Flow field variables at T = 60.

Figure 8.- Structure of time-dependent flow field for subcritical wave; R = 25, $\theta = 60^{\circ}$, $B_o = 1.0$ (BX0 = 0.500, BZ0 = 0.866).

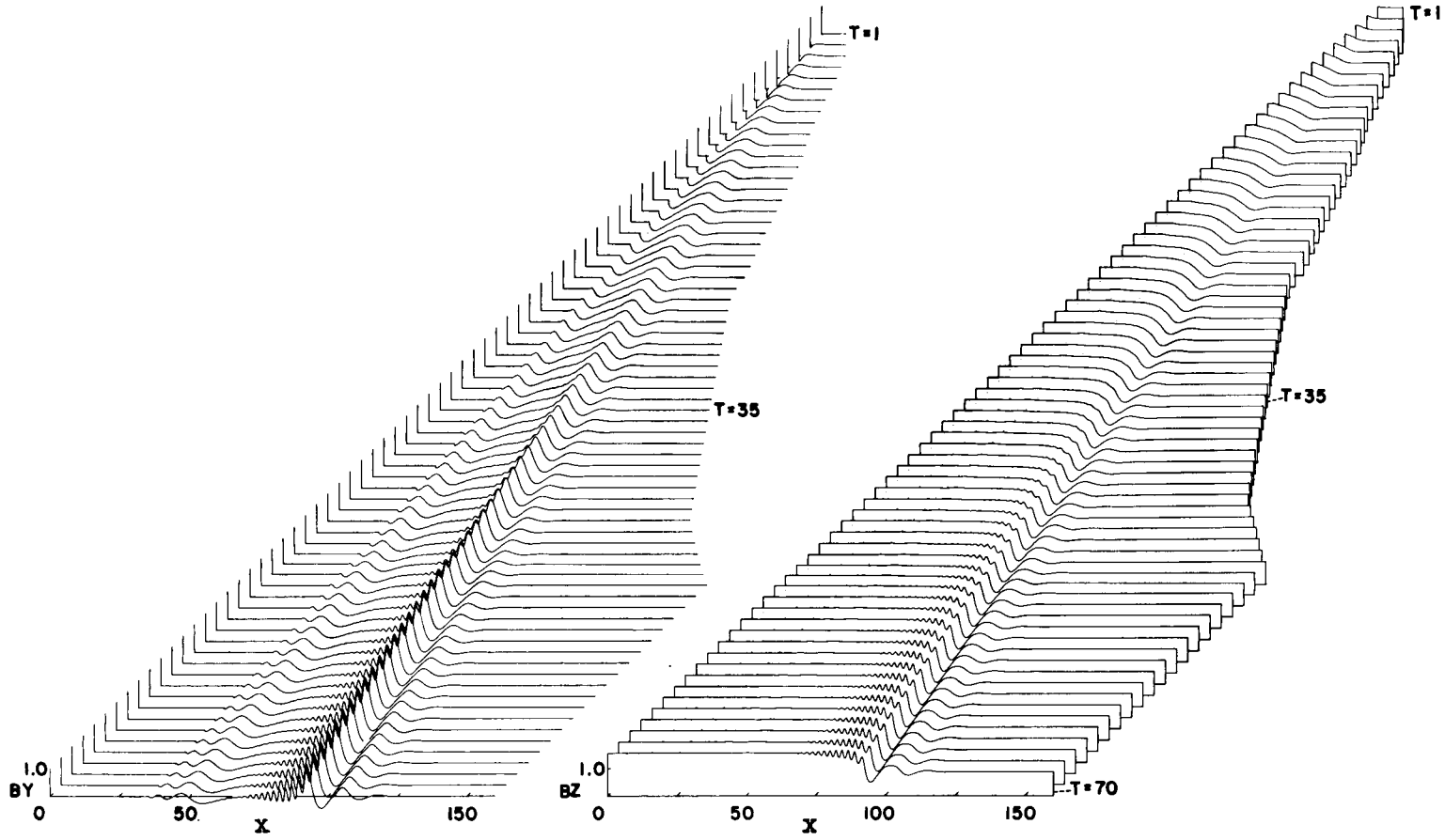

(b) Development of magnetic field components with time. (As with the $\theta = 45^{\circ}$ case, separate wave trains are developing in BY. Now, however, the more fully developed set that is out forward contains a high frequency part. It would be of interest to know whether the second set, growing at the piston-plasma interface, will also develop the high frequency character. If it did not, the initiation of the disturbance field must trigger an oscillation in the leading set not generated in succeeding sets.)

Figure 8.- Concluded.

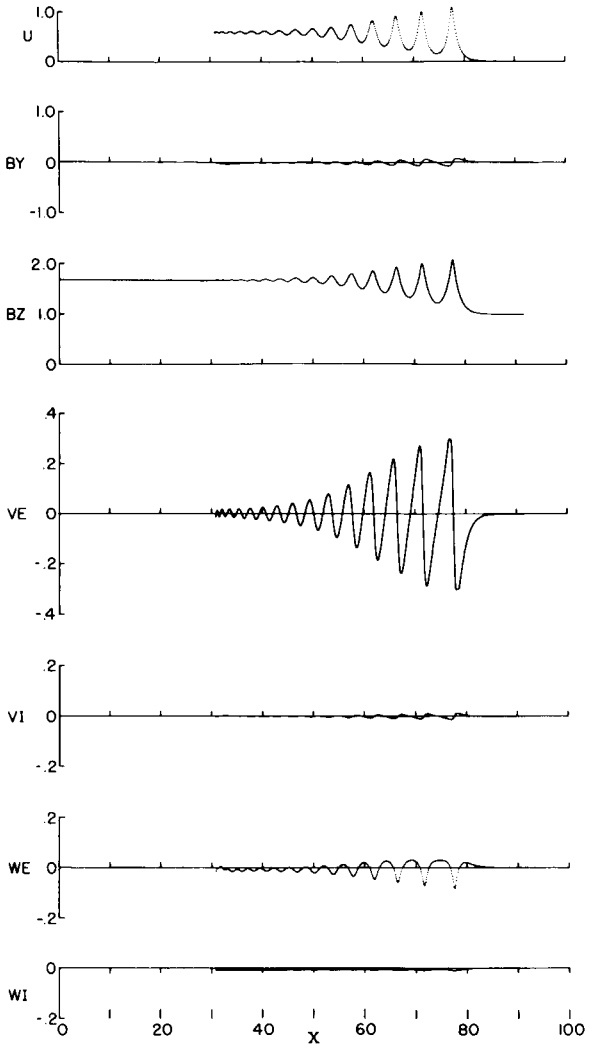

(a) Flow-field variables at T = 60. (Results for this case closely resemble those for $\theta = 90^{\circ}$ (ref. 10).)

Figure 9.- Structure of time-dependent flow field for subcritical wave; R = 25, $\theta = 85^{\circ}$, $B_o = 1.0$ (BX0 = 0.0872, BZ0 = 0.9962).

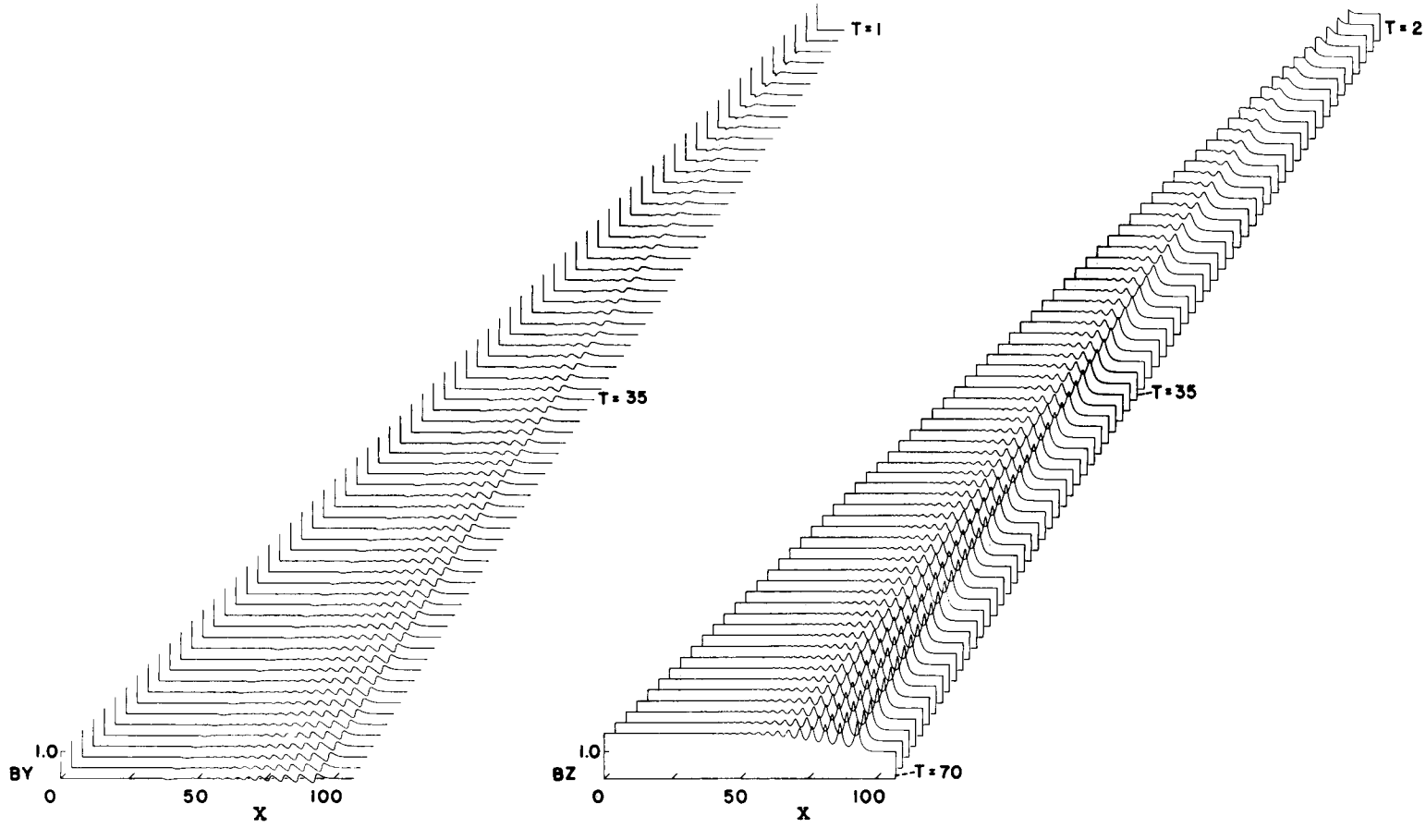

(b) Development of magnetic field components with time.

Figure 9.- Concluded.

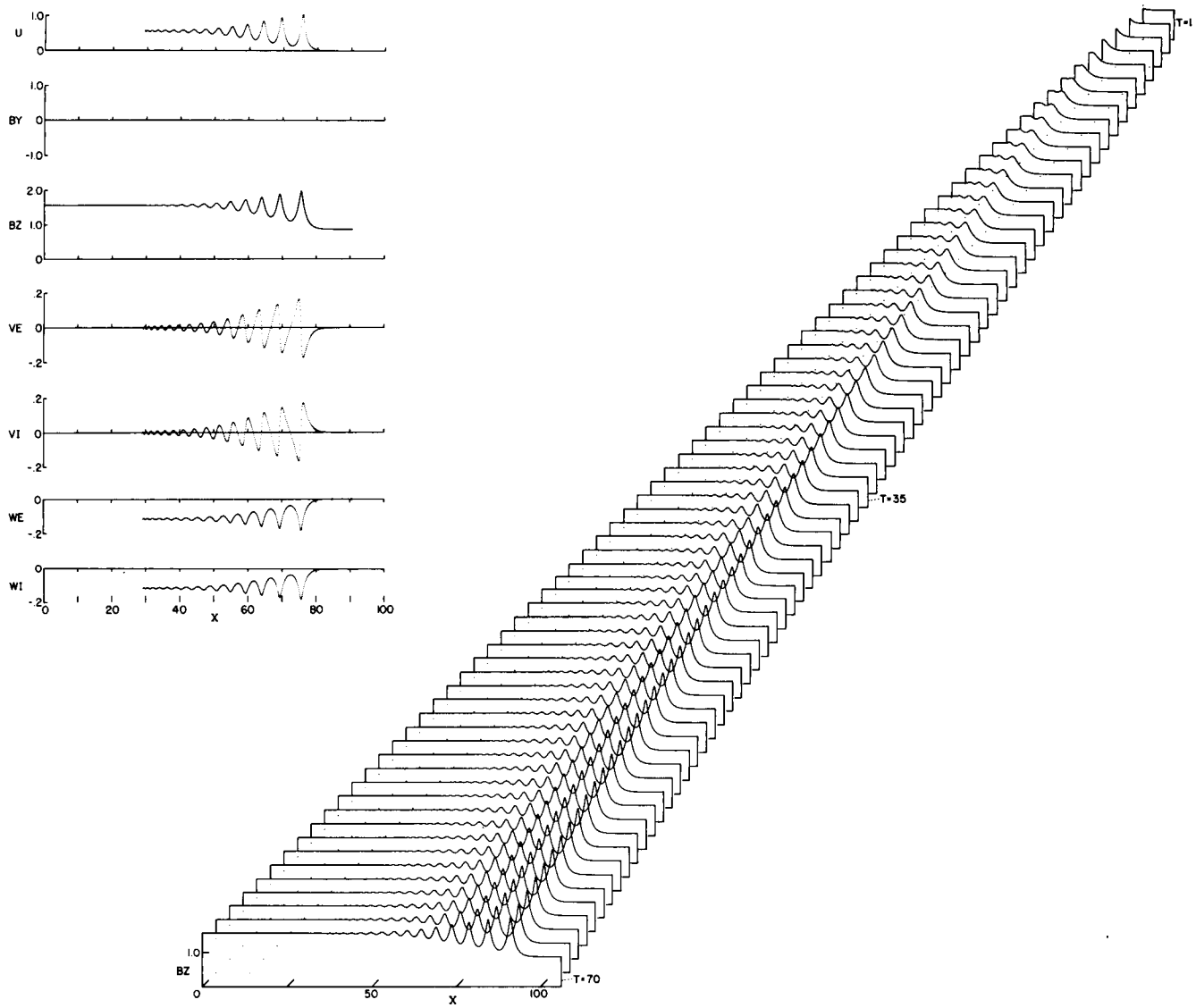

Figure 10.- Structure of time-dependent flow field for subcritical wave; R = 1, $\theta = 60^{\circ}$, $B_o = 1.0$ (BX0 = 0.500, BZ0 = 0.866). (Note that BY = 0, BZ is the same as at $\theta = 90^{\circ}$, and VI = -VE, WI = WE.)

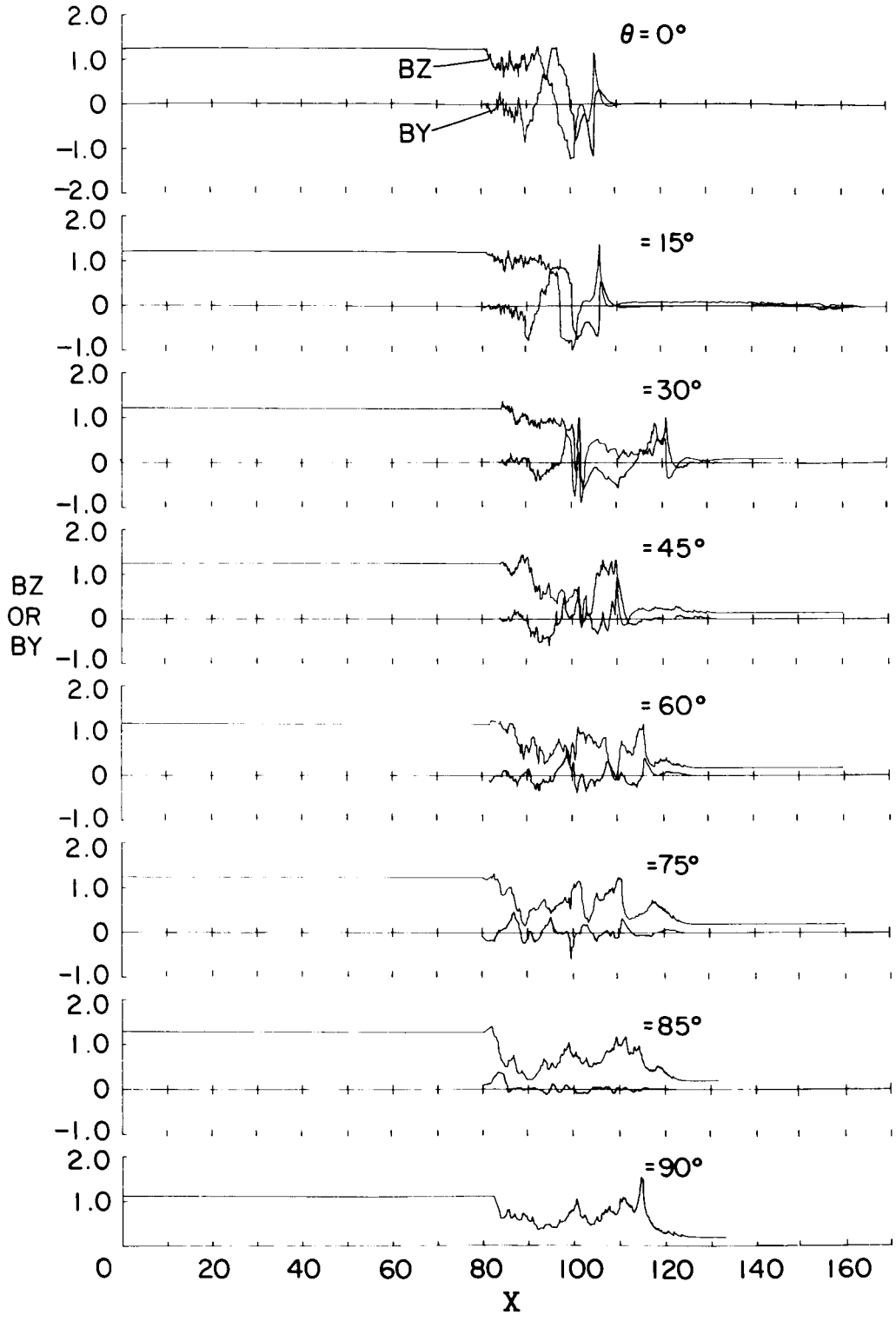

Figure 11.- Structure of compressed layer for supercritical disturbance at several values of magnetic field angle; R = 25, T = 120, B_0 = 0.2 ($M_A \approx 5.8$).

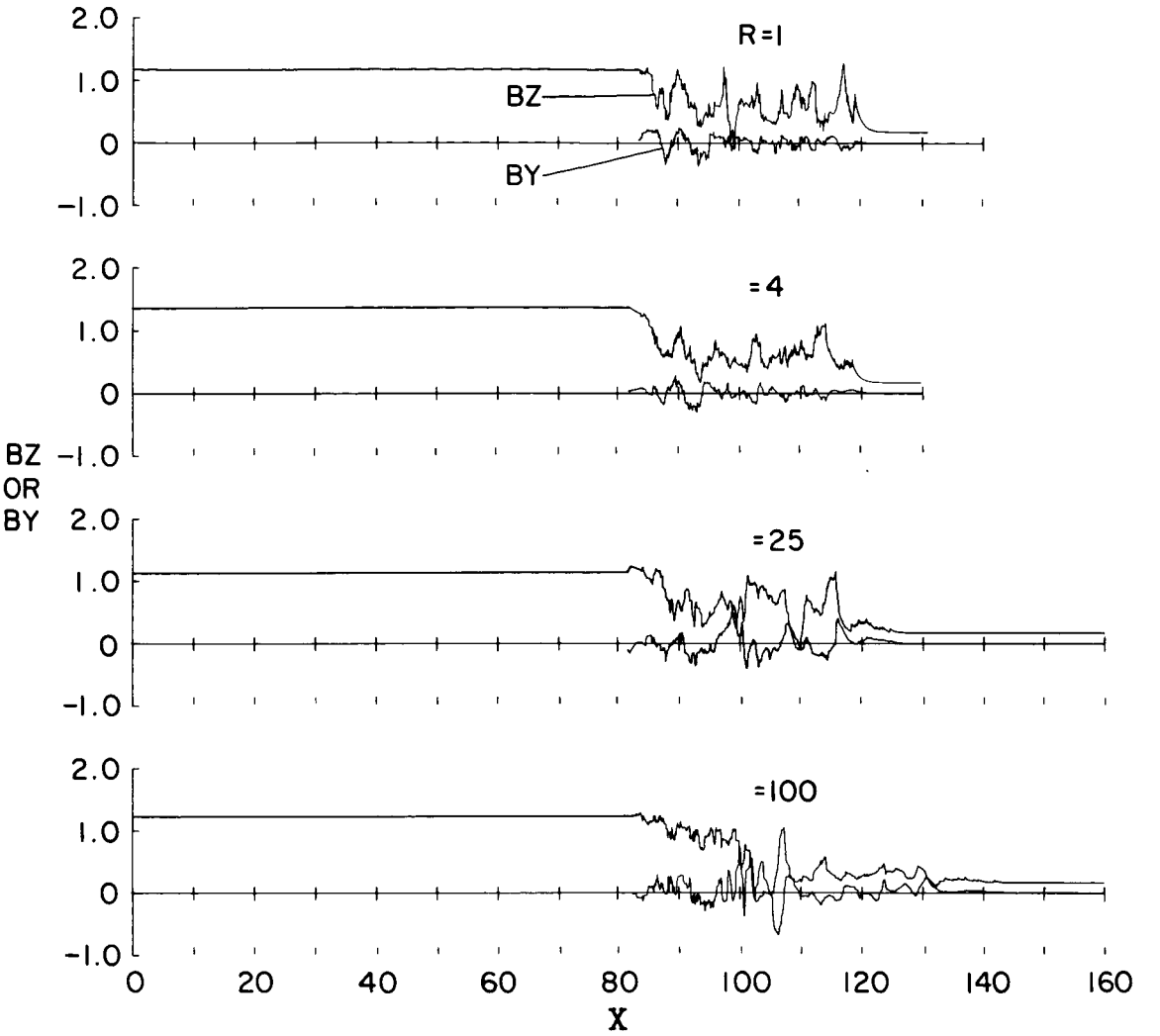

Figure 12.- Structure of compressed layer for supercritical disturbance at various mass ratios; T = 120, $\theta = 60^{\circ}$, $B_o = 0.2$ ($M_A \approx 5.8$).

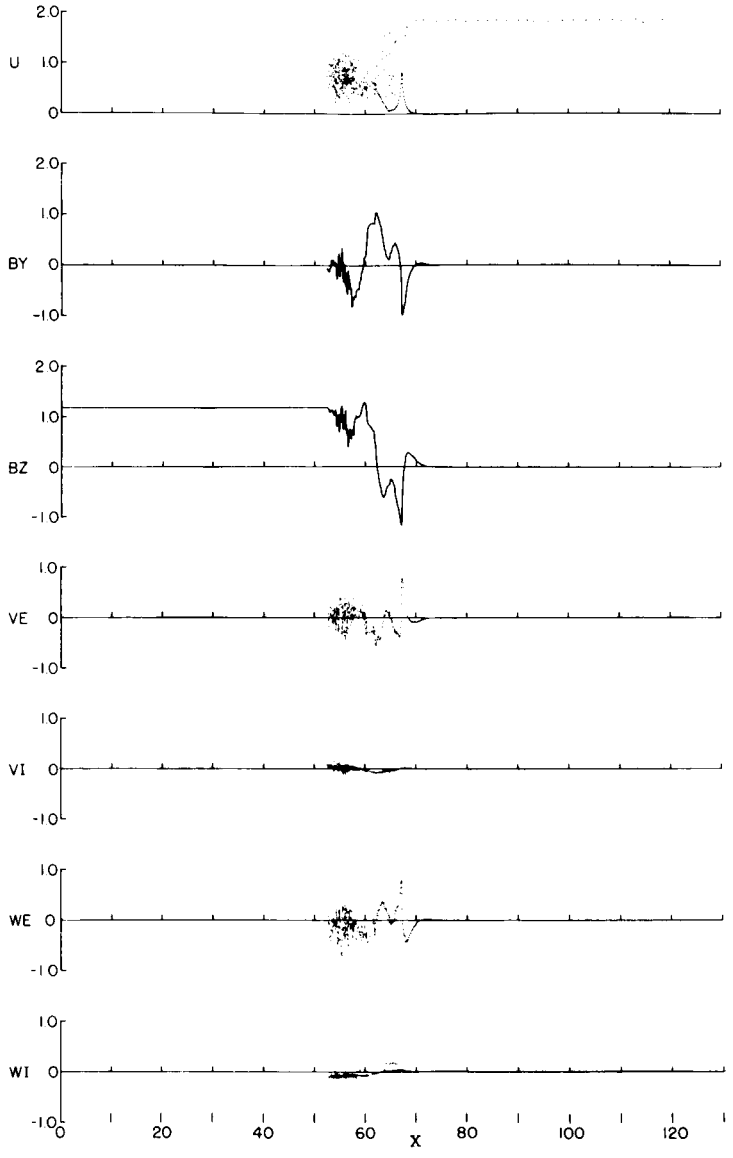

(a) Flow-field variables at T = 60. (Points near $U \approx 2$ in the upper curve are plasma sheets sprayed forward by the rapid initiation of the disturbance field. Such motion of the plasma in the X direction is not inhibited because the transverse magnetic field is zero.)

Figure 13.- Structure of time-dependent flow field for supercritical wave; R = 25, $\theta = 0^{o}$, $B_{o} = 0.2$ (BX0 = 0.2, BZ0 = 0).

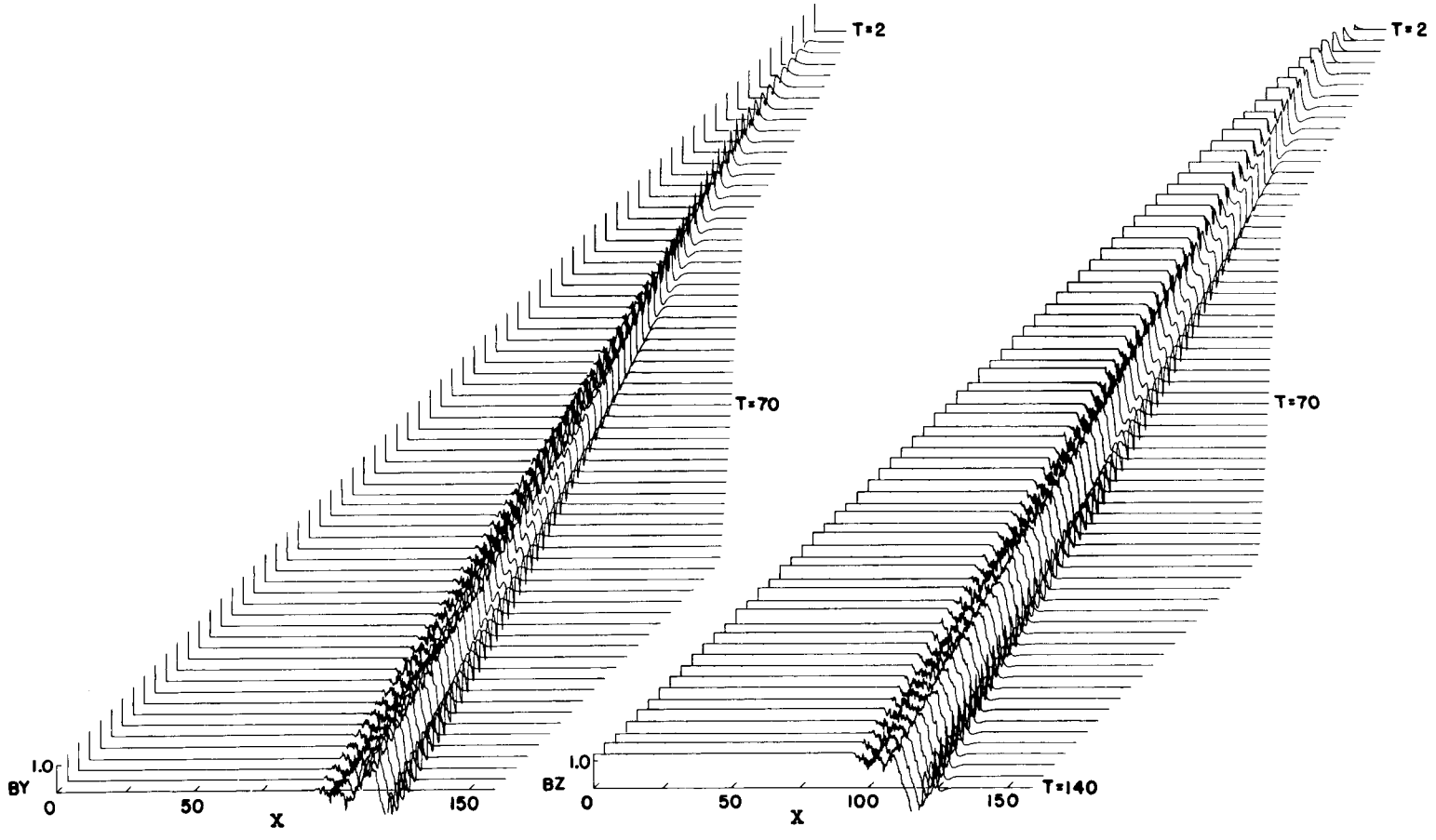

(b) Development of magnetic field components with time. (The time interval between curves is twice that used for the subcritical curves. A nearly uniform compressed layer of thermalized plasma appears to be building up at the piston-plasma interface. It is not certain whether the leading pulse is a solitary type wave or not.)

Figure 13.- Concluded.

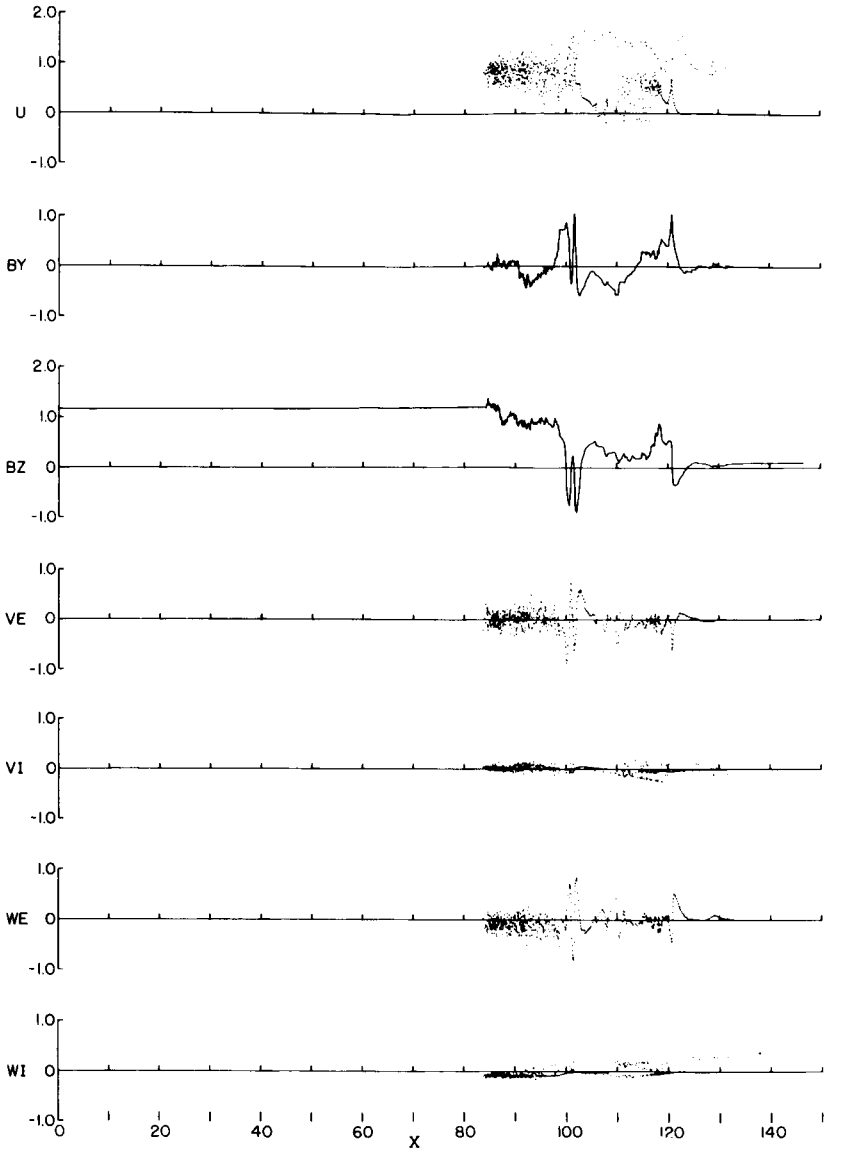

(a) Flow-field variables at T = 120. (A thermalized layer near the piston also builds up in this case. Forward spraying of slabs by the disturbance field at $T \approx 0$ is reduced by the nonzero value of BZ0. Waves in the compressed layer appear to not resemble the solitary waves of Kellogg (ref. 5) so much as the waves typical of $\theta = 90^{\circ}$ (ref. 10).)

Figure 14.- Structure of time-dependent flow field for supercritical wave; R = 25, $\theta = 30^{\circ}$, $B_0 = 0.2$ (BX0 = 0.1732, BZ0 = 0.100).

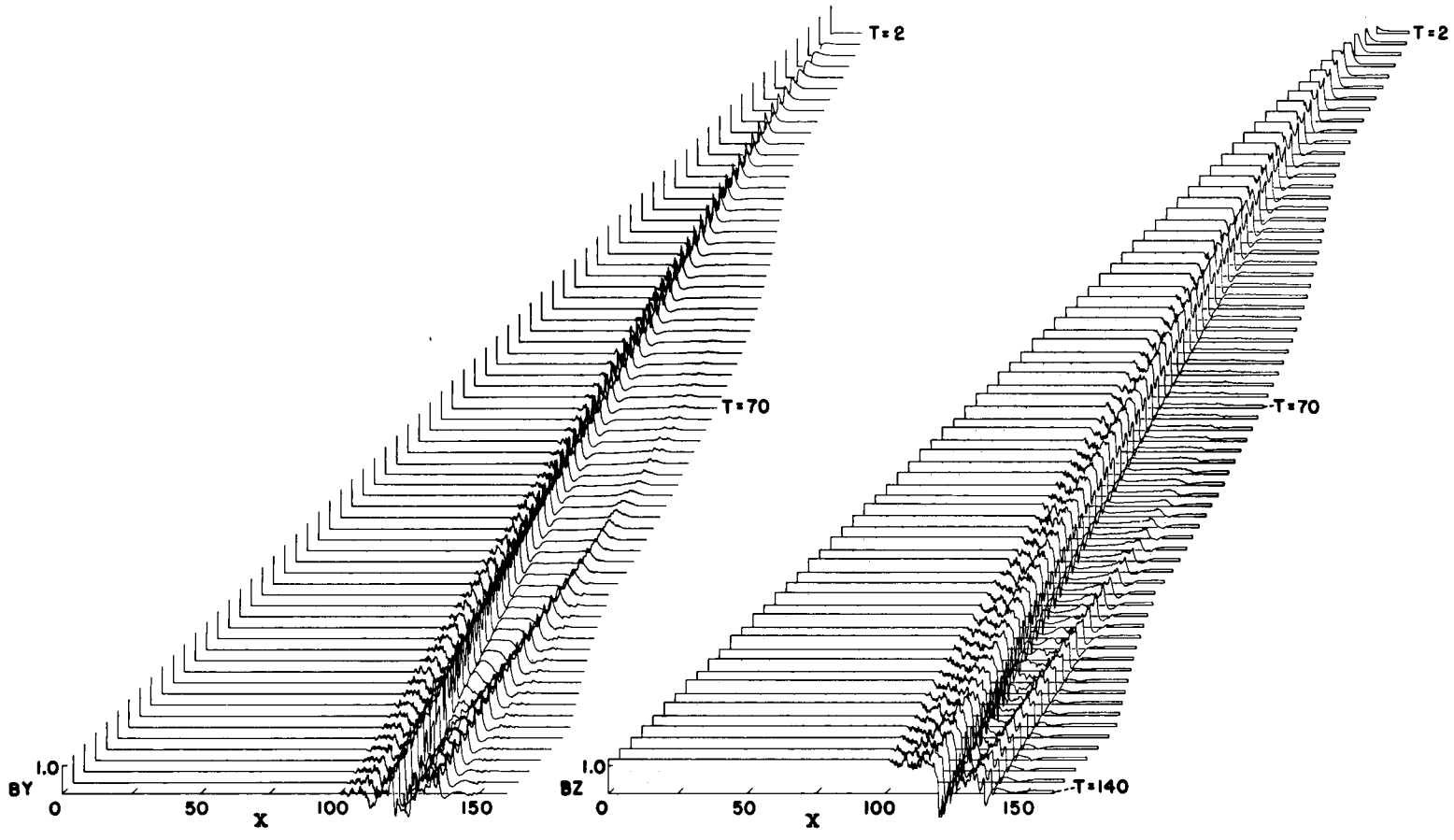

(b) Development of magnetic field components with time. (The compressed layer already appears similar to that at $\theta = 90^{\circ}$.)

Figure 14.- Concluded.

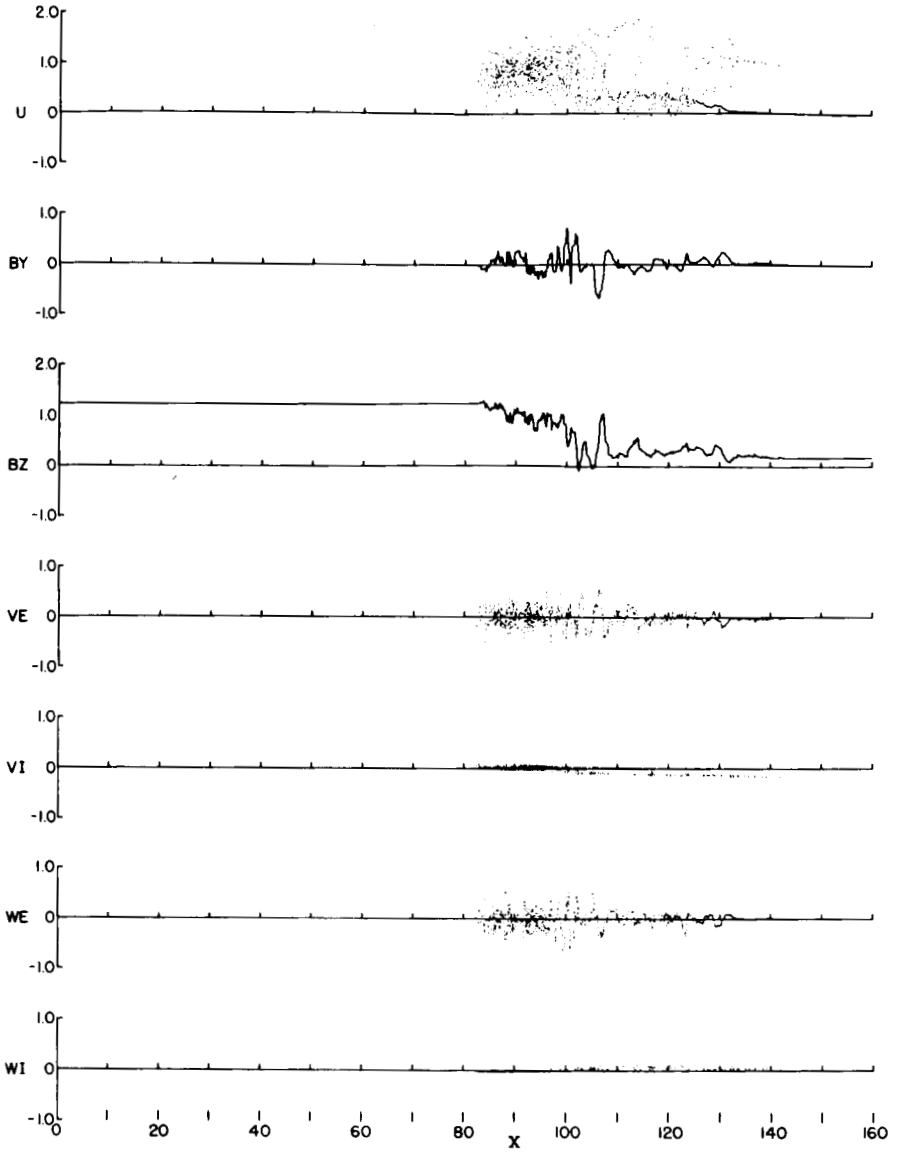

(a) Flow-field variables at T = 120. (The solution is quite similar to that at $\theta = 30^{\circ}$ (fig. 14).)

Figure 15.- Structure of time-dependent flow field for supercritical wave; R = 25, $\theta = 60^{\circ}$, $B_o = 0.2$ (BX0 = 0.100, BZ0 = 0.1732).

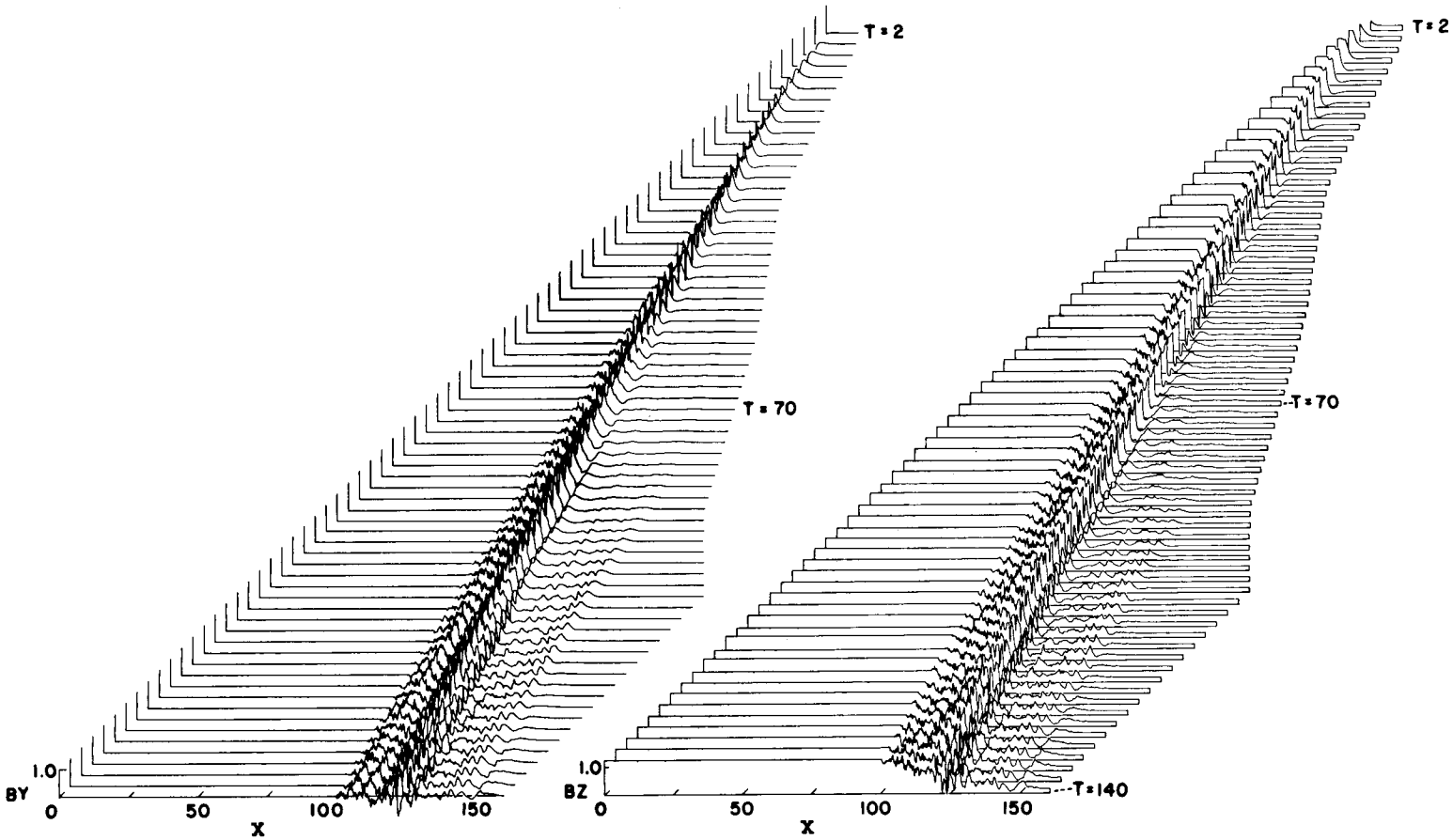

(b) Development of magnetic field components with time. (A nearly smooth wave train ($T \approx 100$-140) that resembles the subcritical solutions leads the chaotic part of the compressed layer.)

Figure 15.- Concluded.

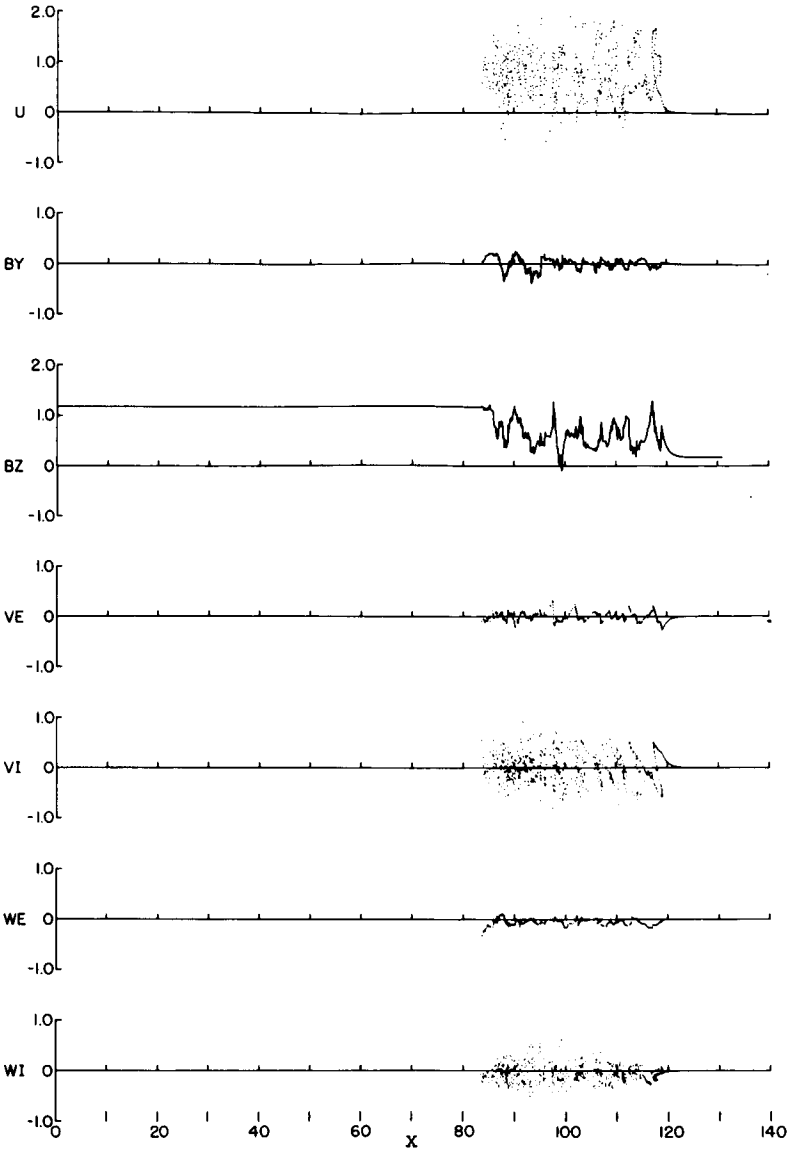

(a) Flow-field variables at T = 120. (Although the compressed layer is nicely thermalized, this solution appears not to reduce to that at $\theta = 90^{\circ}$ as in the subcritical case.)

Figure 16.- Structure of time-dependent flow field for supercritical wave; R = 1, $\theta = 60^{\circ}$, $B_0 = 0.2$ (BX0 = 0.100, BZ0 = 0.1732).

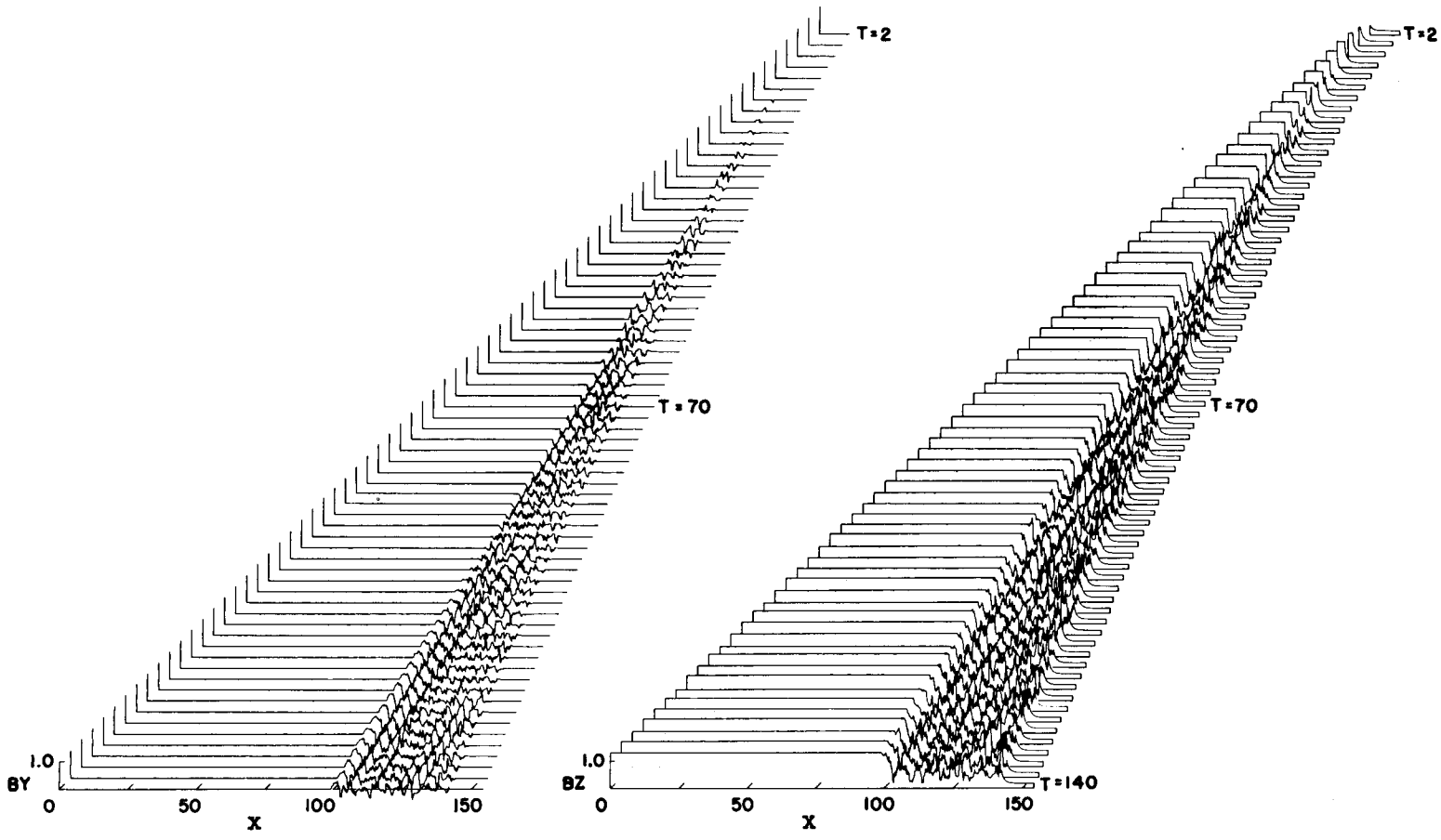

(b) Development of magnetic field components with time.

Figure 16.- Concluded.

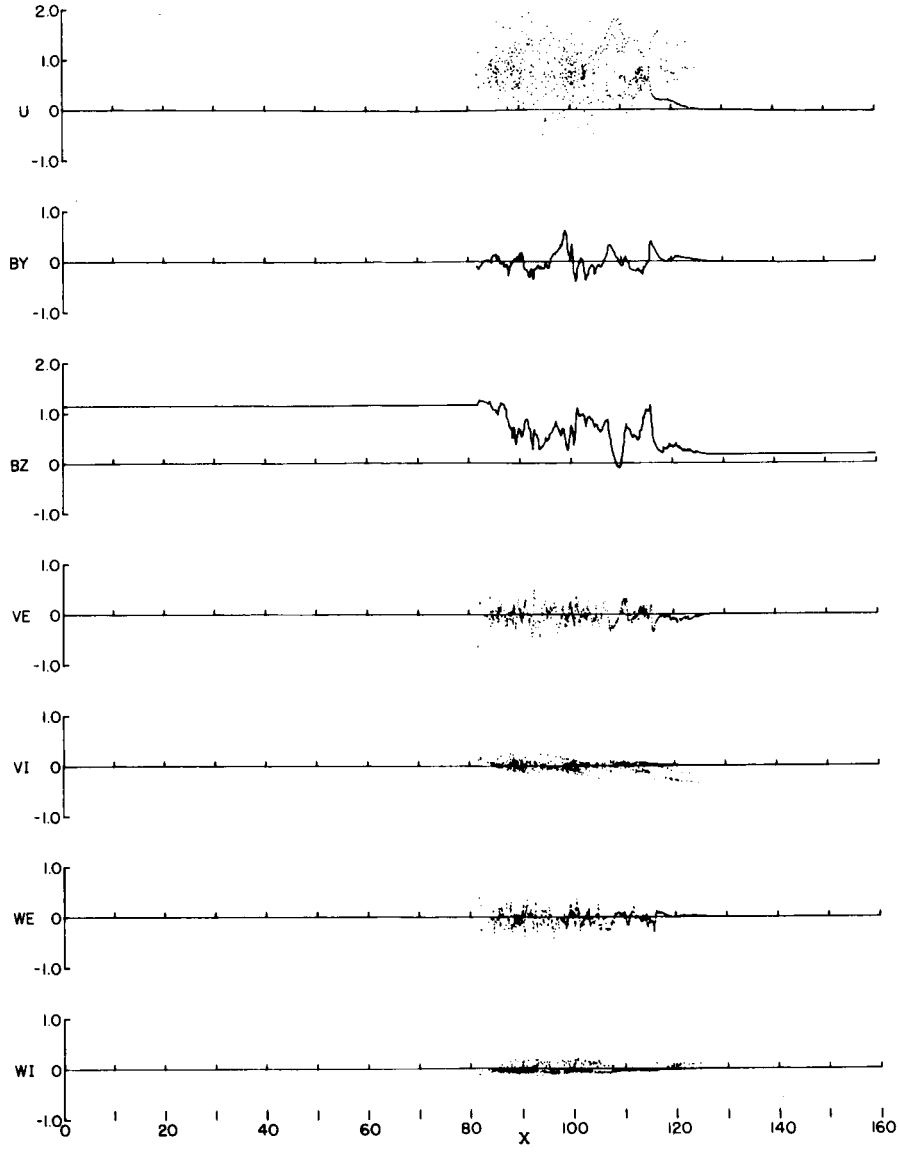

(a) Flow-field variables at T = 120.

Figure 17.- Structure of time-dependent flow field for supercritical wave; R = 100, $\theta = 60^{\circ}$, $B_0 = 0.2$ (BX0 = 0.100, BZ0 = 0.1732).

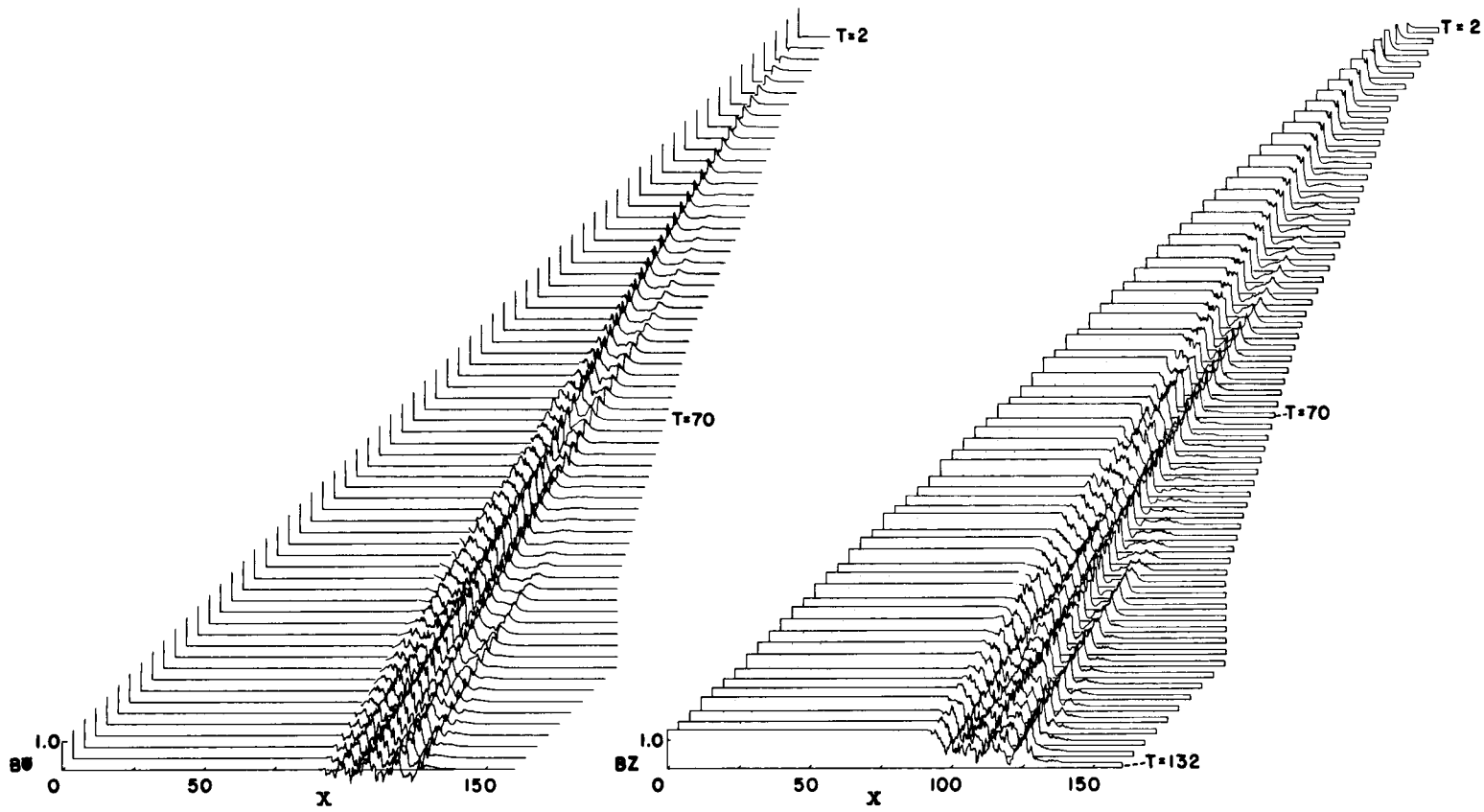

(b) Development of magnetic field components with time. (Appearance of better defined pulses is about all that distinguishes this case from that calculated for R = 1.)

Figure 17.- Concluded.

10-5-67

*"The aeronautical and space activities of the United States shall be **conducted so as to contribute . . . to the expansion of human knowledge** of phenomena in the atmosphere and space. The Administration shall provide for the widest practicable and appropriate dissemination of information concerning its activities and the results thereof."*

—NATIONAL AERONAUTICS AND SPACE ACT OF 1958

NASA SCIENTIFIC AND TECHNICAL PUBLICATIONS

TECHNICAL REPORTS: Scientific and technical information considered important, complete, and a lasting contribution to existing knowledge.

TECHNICAL NOTES: Information less broad in scope but nevertheless of importance as a contribution to existing knowledge.

TECHNICAL MEMORANDUMS: Information receiving limited distribution because of preliminary data, security classification, or other reasons.

CONTRACTOR REPORTS: Scientific and technical information generated under a NASA contract or grant and considered an important contribution to existing knowledge.

TECHNICAL TRANSLATIONS: Information published in a foreign language considered to merit NASA distribution in English.

SPECIAL PUBLICATIONS: Information derived from or of value to NASA activities. Publications include conference proceedings, monographs, data compilations, handbooks, sourcebooks, and special bibliographies.

TECHNOLOGY UTILIZATION PUBLICATIONS: Information on technology used by NASA that may be of particular interest in commercial and other non-aerospace applications. Publications include Tech Briefs, Technology Utilization Reports and Notes, and Technology Surveys.

Details on the availability of these publications may be obtained from:

SCIENTIFIC AND TECHNICAL INFORMATION DIVISION

NATIONAL AERONAUTICS AND SPACE ADMINISTRATION

Washington, D.C. 20546